Universidade de Aveiro

2015

Departamento de Ciências Médicas

Jéssica Sousa Lopes

FTIR, uma potencial ferramenta no diagnóstico de demência através da análise do plasma

FTIR, a potential tool to dementia diagnosis trough analysis of plasma

Universidade de Aveiro

2015

Departamento de Ciências Médicas

Jéssica Sousa Lopes

FTIR, uma potencial ferramenta no diagnóstico de demência através da análise do plasma

FTIR, a potential tool to dementia diagnosis trough analysis of plasma

Tese apresentada à Universidade de Aveiro para cumprimento dos requisitos necessários à obtenção do grau de Mestre em Biomedicina Molecular, realizada sob a orientação científica da Doutora Carla Alexandra Pina da Cruz Nunes, Professora Auxiliar Convidada da Secção Autónoma de Ciências da Saúde da Universidade de Aveiro

Dedico este trabalho aos meus pais pelas oportunidades que me proporcionaram durante toda a minha vida, pois todo o meu percurso académico só foi possível graças a eles. Dedico também à minha irmã por ser a minha companheira em todos os momentos.

o júri

Presidente

Prof. Doutora Odete Abreu Beirão da Cruz e Silva
professora Auxiliar com Agregação do Departamento de Ciências Médicas, Universidade de Aveiro

Professora Doutora Ivonne Delgadillo Giraldo
professora Associada com Agregação do Departamento de Química, Universidade de Aveiro

Professora Doutora Carla Alexandra Pina da Cruz Nunes
professora Auxiliar Convidada do Departamento de Ciências Médicas, Universidade de Aveiro

Agradecimentos

Um agradecimento muito especial à Professora Doutora Alexandra Nunes por todo o apoio, orientação e conselhos que me deu ao longo deste projecto. Um obrigado pela confiança e dedicação prestadas.

Agradeço à Professora Doutora Odete da Cruz e Silva, à Professora Doutora Ana Gabriela Henriques e à Doutora Ilka Rosa pela disponibilização das amostras e dados clínicos.

Agradeço ao Grupo de Investigação de Química Orgânica, Produtos Naturais e Agroalimentares da Universidade de Aveiro, na pessoa da Professora Ivonne Delgadillo por ter permitido a utilização do aparelho FTIR.

Aos meus pais por todo o apoio que me dão em todos os momentos da minha vida. Agradeço-vos por todo o amor que sempre recebi, por me ajudarem a erguer a cabeça nas situações mais difíceis da minha vida. Sem vocês eu não conseguiria atingir todos os meus objectivos.

À minha irmã por estar lá para me ouvir sempre que eu preciso. Por ser a minha grande amiga e confidente.

A toda a minha família, avós, tios e primos pois a família sempre foi o meu grande suporte, por me acompanharem durante a minha vida e por todo o apoio que sempre me deram.

À Alexandra, à Carla, à Catarina, à Helena e à Joana, a segunda família que eu encontrei em Aveiro. Obrigado por todos os momentos que me proporcionaram, sem vocês este meu percurso teria sido muito mais difícil.

A todos os meus amigos por confiarem em mim e por todos os sorrisos que me fazem esboçar.

A Deus, por iluminar sempre o meu caminho e me ajudar a ultrapassar todos os obstáculos.

palavras-chave

Biomarcadores no sangue, demência, diagnóstico, doença de Alzheimer, Fourier Transform Infrared Specctroscopy (FTIR), Infrared Spectroscopy.

Resumo

Atualmente, não é possível fazer um diagnóstico precoce e diferencial da doença de Alzheimer, deste modo, é necessário encontrar biomarcadores que o permitam. Para isso, os cientistas tentam encontrar um procedimento não-invasivo, rápido, e relativamente barato. Os resultados de vários estudos demonstraram que a utilização de técnicas espectroscópicas, tais como a Espectroscopia de Infravermelho Transformada de Fourier (FTIR) e / ou espectroscopia de Raman, podem ser ferramentas úteis para diagnosticar a DA. Uma vez que, na DA, alguns mecanismos bioquímicos podem levar a mudanças em componentes do plasma, podem então ser utilizadas amostras de sangue nas análises espectroscópicas o que torna a técnica simples e menos invasiva.

Com este trabalho pretende-se confirmar algumas das hipóteses de estudos anteriores em que o FTIR foi usado no estudo de amostras de plasma de possíveis doentes com DA e respetivos controlos e verificar a reprodutibilidade desta técnica espectroscópica na análise deste tipo de amostras. Através da análise espectroscopia combinada com análise multivariada é possível discriminar as amostras controlos e dementes e identificar as principais diferenças espectroscópicas entre estes dois grupos de amostras que permitem identificar os metabolitos alterados nesta patologia.

Pode-se concluir que existem três regiões espectrais, 3500-2700 cm^{-1}, 1800-1400 cm^{-1} e 1200-900 cm^{-1} onde se pode extrair informação espectroscópica relevante. Na primeira região, a principal conclusão que é possível tirar é que há um desequilíbrio entre o teor de lípidos saturados e insaturados. Na região entre 1800-1400 cm^{-1}, é possível observar a presença de agregados de proteínas e a alteração na conformação das proteínas para folha β paralela altamente estável. A última região revelou a presença de produtos de peroxidação lipídica relacionados com a insuficiência de membranas, e danos oxidativos nos ácidos nucleicos.

A técnica de FTIR e a informação reunida neste trabalho pode ser utilizada na construção de modelos de classificação que possam vir a ser utilizados para o diagnóstico de disfunções cognitivas.

Keywords Blood-based Biomarkers, Alzheimer's disease, dementia, diagnosis, Fourier Transform Infrared Spectroscopy, infrared spectroscopy.

Abstract

Nowadays it is still difficult to perform an early and accurate diagnosis of dementia, therefore many research focus on the finding of new dementia biomarkers that can aid in that purpose. So scientists try to find a non-invasive, rapid, and relatively inexpensive procedures for early diagnosis purpose. Several studies demonstrated that the utilization of spectroscopic techniques, such as Fourier Transform Infrared Spectroscopy (FTIR) and Raman spectroscopy could be an useful and accurate procedure to diagnose dementia. As several biochemical mechanisms related to neurodegeneration and dementia can lead to changes in plasma components and others peripheral body fluids, blood-based samples and spectroscopic analyses can be used as a more simple and less invasive technique.

This work is intended to confirm some of the hypotheses of previous studies in which FTIR was used in the study of plasma samples of possible patient with AD and respective controls and verify the reproducibility of this spectroscopic technique in the analysis of such samples. Through the spectroscopic analysis combined with multivariate analysis it is possible to discriminate controls and demented samples and identify key spectroscopic differences between these two groups of samples which allows the identification of metabolites altered in this disease.

It can be concluded that there are three spectral regions, 3500-2700 cm^{-1}, 1800-1400 cm^{-1} and 1200-900 cm^{-1} where it can be extracted relevant spectroscopic information. In the first region, the main conclusion that is possible to take is that there is an unbalance between the content of saturated and unsaturated lipids. In the 1800-1400 cm^{-1} region it is possible to see the presence of protein aggregates and the change in protein conformation for highly stable parallel β-sheet. The last region showed the presence of products of lipid peroxidation related to impairment of membranes, and nucleic acids oxidative damage.

FTIR technique and the information gathered in this work can be used in the construction of classification models that may be used for the diagnosis of cognitive dysfunction.

Index

Figures Index

Tables Index

Abbreviations

AD	Alzheimer´s disease
ADDLs	Aβ derived diffusible ligands
ANN	Neural Network Analysis
APPr	Amyloid Precursor Protein Ratio
ATR	Attenuated Total Reflection
BBB	Blood-based barrier
BIOMARKAPD	Biomarkers for Alzheimer´s disease and Parkinson´s disease
CA	Cluster Analysis
CBF	Cerebral Blood Flow
CDR	Clinical Dementia Rating scale
$CMRO_2$	Cerebral Metabolic Rate of Oxygen
CSF	Cerebrospinal Fluid
DLB	Dementia with Lewy bodies
DM	Diabetes Miellitus
DMPC	Dimyristoyl phosphatidylcholine
DTGS	Tryglycine Sulfate
EDTA	Ethylenediamine Tetraacetic Acid
FILD	Frontotemporal Lobar Degeneration
FIR	Far-Infrared region
FTIR	Fourier Transform Infrared Spectroscopy
GDS	Geriatric Depression Scale
Ge	Germanium
HbO	Oxy-hemoglobin
HbR	Deoxy- hemoglobina
HbT	Total-hemoglobin
HTN	Hypertension
IR	Infrared Spectroscopy
KRS-5	Thalium-Iodide
MCT	Mercury Cadmium Telluride
MIR	Mid-Infrared region
MMSE	Mini-Mental State Examination
MS	Mass Spectroscopy
MSI	Metabolomics Standart Initiative
NIR	Near-Infrared region
NIRS	Near-Infared Spectroscopy
NMR	Nuclear Magnetic Resonance
OEF	Oxygen Extraction Fraction
PCA	Principal Component Analysis
PDD	Parkinson´s disease
PLS-DA	PLS Discriminant Analysis
PP2A	Inhibitor-2 of protein phosphatase-2A
PUFA	Polyunsaturated Fatty Acid
SAPC	1-stearoyl-2-arachidonyl phosphatidylcholine
SNR	Signal-to-noise ratio
SVD	Subcortical Vascular Dementia
VaD	Vascular Dementia
ZnSe	Zinc Selenide

Chapters overview

In chapter 1 there is a discussion about the differences between FTIR and FT-Raman spectroscopy and a review about what have been done until now in the area of infrared spectroscopy and dementia diagnosis. This chapter was submitted as a review to the Journal of AD disease.

Chapter 2 gives an overview of FTIR principles and it aims to discuss the intense water contribution in mid-infrared spectrum plasma samples, providing an optimized experimental methodology to overcome this problem.

In chapter 3 will be presented and confirmed previous results on the application of FT-IR spectroscopy to the plasma samples of putative Alzheimer's patients, and age and sex matched controls, in order to identify spectral differences that help discriminate between the two groups.

Chapter 1

1. INTRODUCTION

Diseases associated with age are prone to become increasingly prevalent. According to a WHO report, dementia contributed four 11,2% of the living years with a disability in people over 60 years old – more than stroke, cardiovascular disease and cancer [1–4]. Giving their pathological complexity, it is often difficult differential diagnosis of dementia in clinical practise, and to define landmarks that differentiate dementia from the mild decline in memory and cognitive function seen during ageing. The most common and most debilitating neurodegenerative disorder among the elderly is Alzheimer's disease (AD), which is followed by frontotemporal lobar degeneration (FTLD), vascular dementia (VaD), dementia with Lewy bodies (DLB) and Parkinson's disease dementia (PDD) [5,6].

Nowadays, the available clinical diagnosis criteria used to identify dementia allows to detect pathologies in a very advanced stage of disease, when is too late for any kind of successful disease adjustment. Further, an early and accurate diagnosis of dementia enables detection of potentially treatable disorders that contribute to cognitive impairment, such as depression, vitamin deficiencies and hypothyroidism [7]. It is sorely needed a simple, accurate and cost-effective early diagnosis for dementia in order to treat and even prevent first signs of disease, with introduction of reliable therapeutic approaches (e.g. disease-modifying therapies). This becomes possible with the innovative and different approaches in research that focus on novel dementia biomarkers identification and validation [8,9].

Metabolomic techniques have been used to identify biochemical pathways alterations linked to several diseases, either in biological fluids (plasma, urine and CSF – cerebrospinal fluid), animal models and tissue or cell cultures [10]. Since it allows to identify and/or quantitate the metabolites in a given biological sample, using unbiased metabolomics approach could provide a more complete picture of dementia pathology [8]. The main metabolic fingerprinting techniques for disease diagnosis includes infrared (IR) and Raman spectroscopy, which can provide details of chemical composition and molecular structure of analysed samples. Diseases and other pathological anomalies lead to chemical and structural alterations at the molecular level that also change the vibrational spectra. These spectral changes can be used as sensitive and phenotypic markers of disease, constituting a specific and unique real fingerprint [11,12].

2. POTENTIAL OF BLOOD-BASED BIOMARKERS

CSF represents the most suitable biological fluid to study neurodegenerative diseases since it can reflect the biochemical changes occurring in brain, although its analysis is not always feasible for a large scale screening, because of the huge economic costs and invasive procedures, uncomfortable and not without risk. Besides, CSF is not amenable for repeated sampling that is an important aspect in the perspective of biomarker's role and utility in disease diagnosis and therapeutics. In the other hand, blood-based biomarkers are minimally invasive and could increase diagnostic accuracy, be useful for prognosis and monitoring of therapeutic interventions [13].

It is important to note that only small hydrophobic, lipophilic molecules are more easily transported from CSF into blood, through blood-brain barrier (BBB). This implies that the most relevant markers will be in low abundance in plasma, at least in normal healthy people. Nevertheless, there is increasing evidence for a compromised BBB in neurodegeneration, which will impact on the type of molecules leaking out of brain into blood circulation [2].

One of the main metabolomics challenges for using this approaches in clinical practise is the development of standard protocols regarding sample collection and storage, chemical analyses, data processing, and information exchange. Indeed, it was already created the Metabolomics Standard Initiative (MSI), supported by the Metabolomic Society, to recommend standard protocols for use in all aspects of metabolomic research [14]. Besides, extensive standardization of several aspects of biomarkers analysis is now being addressed through the international quality-control program, which includes CSF reference materials, in the European Joint Programming project “Biomarkers for Alzheimer’s disease and Parkinson’s disease” (BIOMARKAPD) [15,16]. Work to validation of both fluid-based and imaging biomarker thresholds is also ongoing [17].

Since peripheral sources of biomarkers, like blood, are further away from the brain, this implies that peripheral markers will need to be correlated with accepted markers of dementia present in brain tissue and CSF, to demonstrate that these can also reflect dementia pathology [2]. Likewise it is necessary to determine whether these biomarkers can be influenced by other organ systems, since demented patients also typically present comorbidities due to normal ageing process [18].

Other challenge in biomarkers research is the substantial overlap of major brain pathologies, therefore, a better understanding of how combinations of pathologies affect changes in biomarkers is needed [7]. Powerful and innovative bioinformatics tolls will be needed to unravel multivariate plasma disease signatures [2].

3. METABOLOMICS AS A NOVEL APPROACH IN NEW DEMENTIA BIOMARKERS RESEARCH

Metabolomics is an emerging field in development that started to be recently applied as a non-targeted approach to neurodegenerative disorders biomarkers discovery. Metabolomics is now commonly defined as the detection and quantitation of all low-molecular-weight molecules and metabolites present in cells, tissues or organisms under a set of given conditions [2,11,19]. The metabolome is the collection of small molecules that are found within a biological system and whose identities, concentrations and fluxes are the final product of interactions between gene and protein expression, and the cellular environment. Thus, metabolomics information complements the obtained data from genomics, transcriptomics and proteomics [6].

A typical metabolomic study includes four main steps: representative sample collection, sample analysis (e.g. FTIR, nuclear magnetic resonance - NMR, mass spectrometry - MS), statistical analysis (e.g. principal component analysis - PCA, Partial Least Squares- Discriminant analysis - PLS-DA) and identification of significantly altered metabolites that could be translated into new disease biomarkers/pathways, with generation of a disease metabolic fingerprinting [4]. The main metabolic fingerprinting approaches used for disease diagnostics includes IR and Raman spectroscopy, NMR and MS-based methods [20].

Vibrational spectroscopy has been proposed as a reagent-free and non-destructive approach towards tackling the traditional problems associated with biofluids in diagnosis and screening [21]. FTIR has a significant and ongoing history of research into its potential as a diagnostic tool and allows for the extremely rapid, high-throughput and non-destructive analysis of a wide range of sample types. Although FTIR has been previously recognized as not as specific and sensitive as some of the MS-based techniques, the reproducibility of FTIR has been demonstrated through the extensive number of the published research using this technology. Besides, it has been recognized as a valuable tool for metabolic fingerprinting as it is able to simultaneously analyse carbohydrates, amino acids, fatty acids, lipids, proteins, nucleic acids and polysaccharides with a minimum amount of sample preparation. Also, FTIR is less expensive and more accurate rather other methods [11,22]. As a complimentary tool to IR spectroscopy, Raman spectroscopy is also non-destructive, non-contact and reagent-free. Since Raman is a scattering technique and thus it is not perturbed by aqueous, it potentially allow *in vivo* and live-cell imaging. Besides, it has recently been shown that by using centrifugal filter devices to concentrate analytes, an enhanced signal-to-noise ratio (SNR) can be achieved [21].

Apart from several analytical procedures that result in quantitative data, for diagnostic purposes it is important to define some categorical differentiable classes for the obtained data, most commonly by dividing samples in healthy or disease affected classes. This important area of chemometric data processing is called classification, whose main aims are pattern recognition and discrimination analysis. Multivariate analysis uses

mathematical, statistical and computer sciences to efficiently extract useful information from data generated via chemical measurements [23,24]. Multivariate classification techniques can be further divided into two categories: unsupervised and supervised learning procedures. In this first category, it is not required an *a priori* knowledge about training set samples (i.e. the class membership of the training samples), therefore, samples will be grouped into a number of classes with certain communalities without initial qualification of samples and their class assignment. Examples of unsupervised methods are PCA and cluster analysis (CA). Hence, unsupervised patter-recognition techniques are exploratory methods for data analysis, which seek inherent similarities of data. Using this method, unexpected grouping within a training sample set that might not be initially evident may be discovered, e.g. that a group of disease samples might be additionally separated into two or more distinctly different classes [24,25].

4. VIBRATIONAL SPECTROSCOPY: PRINCIPLES AND APPLICATIONS

Spectroscopy has recently arised as one of the major tools for biomedical applications and has made significant progress in the field of clinical evaluation. The vibrational spectroscopic techniques are relatively simple, reproducible, non-destructive to the samples and requires a minimum sample preparation process, with small amounts of biological material (micrograms to nanograms) to spectroscopy analysis [26]. It is important to note that when the drying process is applied to the liquid samples (e.g. plasma), as a method to minimize water signals in spectra, samples restore is impossible after spectroscopic analysis; hence, in this case, vibrational spectroscopy has a destructive nature for samples.

In contrast to other blood products as serum, plasma exhibits a good metabolite concentrations reproducibility, which may result from the simple collecting procedure for plasma, as it does not require time to coagulate [27]. Removal of cellular component from blood, in order to obtain plasma, allows to exclude perturbations of the chemical analysis or to ensure that blood cells metabolism does not interfere with metabolite concentration values. This latter point is particularly important for glucose identification, since its concentration begins to decrease immediately after sampling due to the glycolytic action of erythrocytes and leucocytes [28].

These techniques provide information at the molecular level that allows investigation of functional groups, bonding types, and molecular conformations. Spectral bands in vibrational spectra are molecule specific and provide direct information about the biochemical composition of a given sample, since these bands are relatively narrow, easy to resolve, and sensitive to molecular structure, conformation and environment. Spectral peaks can be often associated with vibration of a particular chemical bond or a single functional group in the molecule [26].

Although Raman spectroscopy and FTIR are relevant techniques with their respective spectra complementary to one another, the two methods differ in the physical mechanism *(Table 1),* showing specific advantages for biological applications [12], [29].

Table 1| Principal technical differences between FTIR and Raman spectroscopy. Adapted from [29].

	FTIR	Raman
Type of samples	mainly non-aqueous	both aqueous and non-aqueous
Main analysis troubles	strong absorption bands of water	fluorescence and strong effect of glass
Sample preparation	more than Raman	Minimal
Confocal imaging	cannot perform	can perform
Physical effect	changes in dipole moment during molecular vibration (dipole and ionic bands)	change in polarizability (covalent bands)
Resolution	lateral: 1-2 µm; confocal: 2,5 µm	lateral: 10-20 µm

Instrumentation is thus typically less complex for IR (absorption of radiation) than for Raman (light scattering). Besides IR data collection is usually faster, often leading to higher SNR than those obtained through Raman. In the other hand, aqueous systems can only be analysed by IR spectroscopy if samples of few micrometre thickness are prepared (for tissue samples) or if attenuated total reflection (ATR) measurements are performed [12]. ATR-FTIR spectroscopy may cover a relatively large sampling area, which makes it an ideal technique for cytology as large numbers of cells can be studied at given time, becoming easier to identify a small number of atypical cells. Also, since dispersion effects are weaker in ATR-FTIR, there are fewer spectral artefacts. This makes from ATR-FTIR a very applicable method to the routine monitoring of biofluids [21].

IR spectral region *(Figure 1)* ranges from the red end of visible spectrum at 780 nm (12820 cm^{-1} of wavenumber) to the onset of microwave region at a wavelength of 1 mm (10 cm^{-1}). In turn, IR range is further subdivided into the near-infrared (NIR), mid-infrared (MIR) and far-infrared (FIR) regions. MIR covers the range 4000-400 cm-1 and is the region that usually provides the fingerprint characteristics of molecular species, especially at 1500-600 cm^{-1} (fingerprint region). Raman spectroscopy generates bio-fingerprint spectra within the 2000-400 cm^{-1} region, and it is based on inelastic light scattering of monochromatic light from a laser in the visible, NIR or near-ultraviolet regions [21], [30].

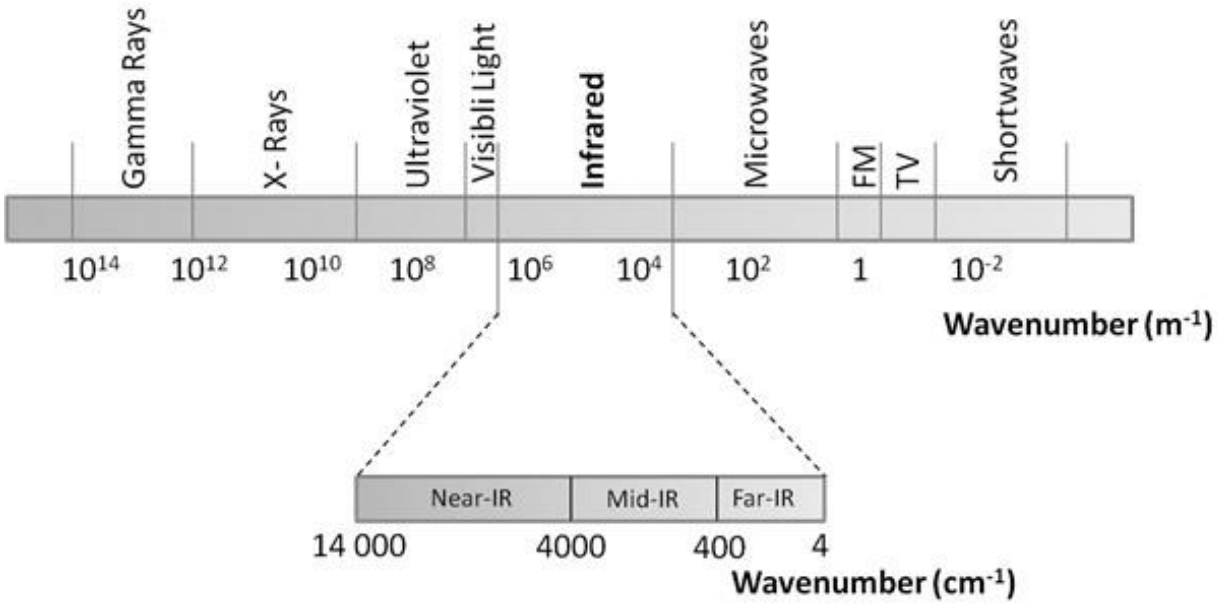

Figure 1|The electromagnetic spectrum, with IR region magnified. Adapted from [31], [32].

Protein misfolding and aggregation are present at a range of neurodegenerative diseases, including certain forms of dementia such as AD and PDD, whereby a secondary structure change of specific proteins into β-sheet enriched conformations occurs. FTIR is also a powerful tool to determine such secondary structure alterations, which can potentialy be used as diagnostic markers. Given the challenge of secondary structure analysis of a specific protein within a complex body fluid, it was developed a novel ATR-FTIR based immune-sensor, whose main element is an ATR-flow-through cuvette equipped with a germanium crystal as an internal reflection element. This cuvette is covered with a quartz-window that allows parallel control-measurements by fluorescence spectroscopy. According to Nabers et al. 2015 that developed this methodology using Aβ peptide, the sensor has to be optimized with a highly-specific Aβ-antibody (process of sensor surface modification). Nevertheless, it is a new hope for label-free diagnostics in complex body fluids [33].

Ultimately, it will be needed an easy-to-use analytical tool, using validated classification or biomarker analysis system, allowing for on-the-spot repeat measurements at minimal cost. Such a microfluidic device would only require a small aliquot of blood, which could be separated into plasma or serum; directed to independent ATR diamonds, a spectral reading could then be remotely classified giving an answer within minutes or seconds. Hence, monitoring of emerging disease, it would likewise open doors for a more personalized medicine [21].

5. FT-RAMAN AND FTIR APPLIED TO DEMENTIA DIAGNOSIS

Some studies have been conducted using FTIR and FT-Raman supporting the use of these techniques in the diagnosis of certain dementias. Promising results have been obtained with different groups reporting similar data as summarized below.

The results obtained by P. Carmona et al. 2012, using FTIR, about the amide I band mean spectra shows differences in the 1640–1625 cm^{-1} range, the local where protein β - amyloid can be detected, between the group of controls and the group of patients with moderate AD. In this range, it was detected an increase in the intensity of the AD spectrum at 1631 cm^{-1} and 1638 cm^{-1}, the first one related to the development of amyloid β-sheet structures and the second to the β-sheet proteins, which generate amide I vibrational modes clustering. Another peak at 1683 cm^{-1} was also related to the β-sheet structure and all these differences can be evidence that AD can be related with oxidative stress. Auto-peak at 1730 cm^{-1} was associated to carbonyl absorption; the auto-peaks appearing near 1656 and 1665 cm^{-1} can be related to α-helices and turns, respectively; and the auto-peak at 1642 cm^{-1} demonstrate that those structures can change to β-sheet and/or unordered structure [34].

Another study of P. Carmona et al. 2013 that compares the controls and moderate AD samples, using Raman spectroscopy, showed an increase in the intensity at 1672 cm^{-1} and a decrease at 1658 cm^{-1}. The increase at 1672 cm^{-1} could be caused by β-sheet-rich proteins or peptides such as $A\beta_{1-40}$ and $A\beta_{1-42}$. In AD samples an increase in the intensity of the 409 cm^{-1} band comparing with controls could also be observed. This band was likewise associated with $A\beta_{1-40}$ and $A\beta_{1-42}$ peptides. The authors correlate the decrease in the intensity at 1658 cm^{-1} with a decrease in the intensity at 980-910 cm^{-1} in the AD spectrum, proposing that this could be related to α-helices. In the map of the FTIR spectroscopy it was observed two correlated peaks, the strongest at 1635 cm^{-1} and another at 1690 cm^{-1}, these peaks are related to protein β-sheets. About the tertiary structure of the proteins the results showed alterations in the AD spectral range at 780–730 cm^{-1}, associated with an increase of band intensity near 758 cm^{-1} and other near 743 cm^{-1}. The first one caused by the indole ring-breathing vibration of tryptophan residues and the second band is due to the in-phase benzene CH out-of-plane bending vibration. The map of FTIR can also indicate markers of oxidative stress in AD. In this report an auto-peak ranging from 1120 to 1000 cm^{-1}, one at 1235 cm^{-1} and other at 1295 cm^{-1} correlating to oxidative stress signal were observed. The cause of the first one can be the C-O stretching vibrations, while the second one is caused by protein β-sheets and both are correlated, the third peak is negatively correlated with the second because it is attributed to α-helices [35].

An additional study by E. Ryzhikova et al. 2014, appling Raman technique, that could differentiate AD from healthy controls showed 7 different regions (13 bands). The first region was located at 400–467 cm^{-1} and exhibit three different bands (at 415, 419 and 455 cm^{-1}), corresponding to proteins, lipids, carbohydrates, phosphatidylinositol and

phosphoenolpyruvate. The second region was located at 505–523 cm^{-1}, and presented bands at 509, 519 and 526 cm^{-1}, related to proteins, carbohydrates, coenzyme A, phosphatidylinositol, phosphatidylserine, acetoacetate and glutathione. The third region was located at 993–1011 cm^{-1}, with one band at 1003 cm^{-1} correlated to proteins, carbohydrates and acetoacetate. The fourth region, located at 1030–1049 cm^{-1} was represented by two bands at 1031 and 1050 cm^{-1} that corresponds to proteins, carbohydrates, fatty acids, phosphoenolpyruvate and coenzyme A. The fifth region was located at 1218–1237 cm^{-1} and has two bands (at 1207 and 1235 cm^{-1}) related to proteins and pyruvate. The sixth region wwas located at 1444–1462 cm^{-1}, the band identified was located at 1448 cm^{-1} and was correlated to proteins, fatty acids, carbohydrates, phosphoenolpyruvate, acetoacetate, β-carotene and glutathione. The seventh region was located at 1537–1556 cm^{-1} with one band at 1553 cm^{-1} that was related to guanine, tryptophan, proline, palmitic acid and N-acetylglucosamine [36].

Further, P. Chen, Q. Tian, et al. 2011 reported that the Raman spectra exhibited two principal differences between the spectra of the controls and the spectra of two AD models (4-month and 12-month old AD transgenic mice), namely at 740 and 1654 cm^{-1}. The first peak showed an increased in intensity, comparing the controls with the AD mice, which could be probably caused by alterations in the amyloid precursor protein ratio (APPr). The peak at 1654 cm^{-1} presented a decrease in the intensity that was probably related to amide I band of the protein α-helix structure [37].

Regarding in dementia diagnosis, of E. Peuchant et al. 2008, reported three regions that could help in AD diagnosis. One is located at 1480 – 1140 cm^{-1} and presented six peaks: 1455 cm^{-1}, due to the CH_2 bending vibrations of mainly fatty acids; 1402 cm^{-1} related to the COO- symmetric vibrations of amino acid side chains and fatty acids; 1343 and 1315 cm^{-1}, correlated to the CH2 side chain vibrations in lipids and proteins; 1242 and 1155 cm^{-1}, caused by the asymmetric phosphate stretching vibrations and by the stretching vibration of the CO group of the nucleic acid ribose. A region between 1140 and 1095 cm^{-1} were three peaks at 1128, 1119 and 1105 cm^{-1} were observed are linked to the phosphate stretching vibrations of the phosphodiester backbone and the stretching vibrations associated with the CO group of deoxyribose. Another peak was associated with the CO stretching vibrations in deoxyribose/ribose of nucleic acids at 1053 cm^{-1}. Third region was located between 1020 and 930 cm-1 and five peaks, related to the CO stretching vibrations in osidic acid and protein structures and to the symmetric stretching mode of dianionic phosphate monoester of nucleic acids, were detected at 1012, 994, 987, 970, and 936 cm^{-1} [38].

Additional, results of some IR spectroscopy studies of isotopically labeled Aβ10–35′ and $A\beta_{40}$ showed an amide I band maximal at 1658 cm^{-1} for unlabeled or 13C-labeled forms of $A\beta_{40}$, the results are similar for unlabeled or labeled forms of Aβ10–35′. For unlabeled $A\beta_{10-35'}$ and $A\beta_{40}$ after aggregation the amide I band is maximal at 1624 cm^{-1} and has a high frequency shoulder at 1685 cm^{-1}. PATIR-FTIR (polarized attenuated total internal reflection-FTIR) spectra of Aβ42 on monolayer membranes made from 100%

DMPC (dimyristoyl phosphatidylcholine) or oxidatively damaged SAPC (1-stearoyl-2-arachidonyl phosphatidylcholine) revealed a common feature in both membranes at ~1623 cm^{-1} and probably due to membrane-adsorbed Aβ42 in a β-sheet conformation. Another component at ~1650 cm^{-1}, that was less evident, indicates that some of the adsorbed protein has a helical or random coil structure. The conclusion of these data was that Aβ42 acquire an antiparallel β-structure induced by an oxidized damaged membrane. The IR spectroscopy it was also used to study the capacity of Aβ42 to seed fibril formation by Aβ40 and it was observed that this ability of Aβ42 only occurs on membranes containing oxidatively damaged SAPC [39].

Concerning the results of the aforesaid study of E. Ryzhikova et al., at differentiating AD from other types of dementia, were obtained 9 regions of interest (30 bands), as described in *(Table 2).*

Table 2|Raman spectral regions and bands of interest, with respective sample contents. Adapted from [36].

Regions	Bands	Sample contents
410–672 cm^{-1}	415, 419, 455, 477, 509, 519, 526, 545, 567, 585, 605, 621, 643 and 662 cm^{-1}	proteins, lipids, carbohydrates, riboflavin, phosphatidylinositol and phosphoenolpyruvate
710–784 cm^{-1}	718, 744 and 757 cm^{-1}	proteins, phospholipids, phosphatidylcholine, phosphoenolpyruvate, acetoacetate, coenzyme A, acetyl coenzyme A, D-fructose-6-phosphate, riboflavin and glutathione
973–1010 cm^{-1}	1003 cm^{-1}	proteins, carbohydrates and acetoacetate
1086–1122 cm^{-1}	1083, 1104 and 1126 cm^{-1}	proteins, carbohydrates, acetyl coenzyme A, acetoacetate, D-fructose-6-phosphate, phosphoenolpyruvate and phospholipids
1199–1235 cm^{-1}	1207 and 1235 cm^{-1}	proteins and pyruvate
1311–1348 cm^{-1}	1317 and 1338 cm^{-1}	Proteins, carbohydrates, phosphoenolpyruvate, glutathione and phospholipids
1424–1498 cm^{-1}	1448 cm^{-1}	proteins, fatty acids, carbohydrates, phosphoenolpyruvate, acetoacetate, β-carotene and glutathione
1537–1611 cm^{-1}	1553 and 1586 cm^{-1}	guanine, tryptophan, proline, lysine, palmitic acid and N-acetyl –glucosamine
1649–1800 cm^{-1}	1657 cm^{-1}	proteins, amide I, α-helix and phospholipids

Raman and NIR spectroscopy are also used to study other types of dementia, such as PDD, Schipper, Kwok, Rosendahl et al 2008. For Raman spectroscopy it was observed an

increase in the alcoholic (R-OH) and nitrogenous (N-H) scatter bands at 3330 and 3200 cm^{-1}, respectively, also accompanied by the detection of a decrease in the hydrocarbon (C-H) scatter at 2990 cm^{-1}, comparing the controls with the PD patients. This technique aided in PDD diagnose with a specificity of 72% and a sensitivity of 74%. The results obtained for NIR were similar with the ones mentioned before; a band at 700 nm corresponds to background, one at 830 nm related to C-H, one at 942 nm due to R-OH, one at 983 nm correlated to water vibrations and one at 1014 nm due to N-H [40].

One of the applications of NIR spectroscopy is in the analyses of some changes in the concentrations of oxy-hemoglobin (HbO), deoxy-hemoglobin (HbR) and total-hemoglobin (HbT). To study these changes in patients with Subcortical VaD the researchers combined two techniques NIR spectroscopy and fMRI (functional magnetic resonance imaging). With these hemodynamic results it was possible to evaluate cerebral blood flow (CBF) and cerebral metabolic rate of oxygen (CMRO2) in individuals with Subcortical VaD. The Study showed a decrease in $CMRO_2$, CBF and in flow-metabolism coupling ratio and an increase in the oxygen extraction fraction (OEF) [41].

6. FTIR ANALYSIS OF BLOOD-BASED SAMPLES

As mentioned, direct analysis of an FTIR spectra *(Figure 2)*, permits the identification of the maximum wavenumber peaks. Each of these spectral signals have one or more assignment (specific type of molecular vibration), that corresponds to a certain chemical group and/or chemical family of compounds. This correspondence allows to establish a specific chemical pattern of analysed samples, with identification of the main chemical components *(Table 3)*. Figure 2 represents the model spectra of a plasma sample, at 4000-600 cm^{-1} region, showing maximum wavenumber peaks obtained in this study, the samples were dried.

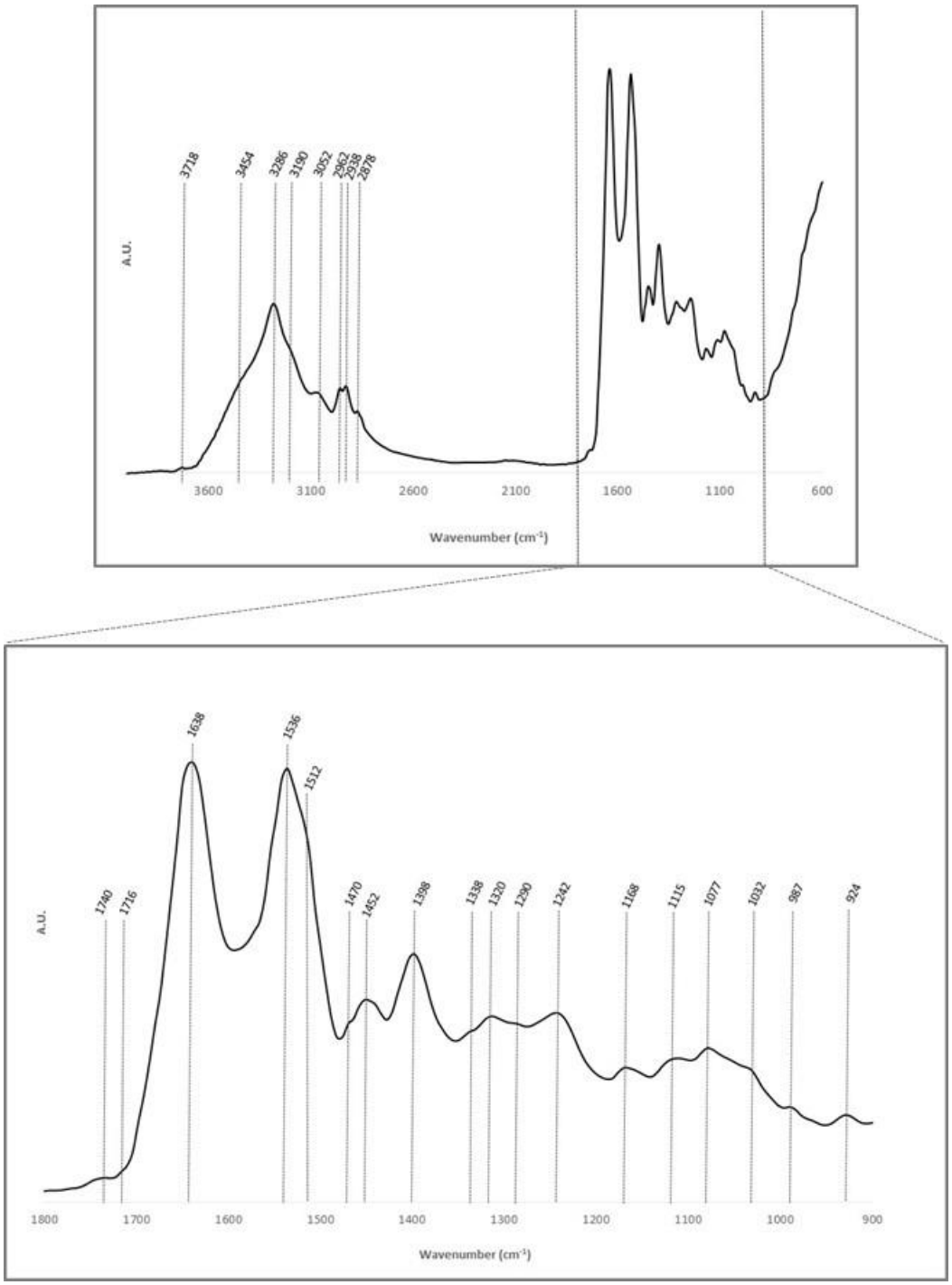

Figure 2| FTIR model spectra of a plasma sample, at 4000-600 cm^{-1} region, showing maximum wavenumber peaks. The downer picture is a magnification of the 1800-900 cm^{-1} spectral region acquired from the first spectra, showing also maximum wavenumber peaks. X-axis: wavenumber (cm^{-1}); Y-axis: arbitrary units (A.U.)

Table 3| Maximum wavenumber peaks founded in FTIR spectra and its main assignments and correspondents plasma contents.

Peaks (cm^{-1})	Assignments	Plasma contents	Ref.
≈ 3718	O-H stretching and an intermolecular vibration of CO_2 and phenol**	Presence of gaseous CO_2	[42]
≈ 3454	N-H stretching	Proteins (amide A)	[43]
≈ 3286	N-H stretching, H-O-H symmetric and asymmetric stretching*	Proteins (amide A)	[44], [45]
≈ 3190	N-H symmetric stretching	mainly cis-ordered sub-structures	[26]
≈ 3052	N-H stretching	Proteins (amide B)	[26]
≈ 2962	C-H asymmetric stretching of CH_3 group*	Lipid acyl chains in lipid bilayers (phospholipids)	[29], [44], [46], [47]
≈ 2938	C-H stretching of CH_2 and CH_3 group*	Fatty acids	[29], [43], [44]
≈ 2878	C-H symmetric stretching of CH_3 group*	Lipid acyl chains in lipid bilayers (phospholipids)	[29], [44], [46], [47]
≈ 1740	C=O stretching	Fatty acid esters (triglycerides), lipid bilayers (phospholipids)	[23], [44], [46]
≈ 1716	C=O stretching	Carbonic acid, phospholipid sub-structures, purine bases from nucleic acids	[23], [29], [44], [48]
≈ 1638	C=O stretching*; NH_3^+ asymmetric in plane bending (rocking)*	Proteins (amide I for β-sheet); Membrane lipids (phospholipids)	[29], [44], [47], [49]
≈ 1536	N-H bending in plane, C-N stretching*	Proteins (amide II)	[29], [44], [45]
≈ 1512	CC (phenyl ring) stretching, CH in plane bending*	tyrosine band (proteins side chain)	[29], [44], [50]
≈ 1470	CH_2 bending; C-H asymmetric bending; CH_2 symmetric in plane bending (scissoring)*	Proteins; Carbohydrates; Lipid acyl chains in lipid bilayers (phospholipids)	[23], [26], [29], [47]
≈ 1452	CH_2 bending and CH_3 asymmetric in plane bending (rocking)*; C-O symmetric stretching	Proteins, membrane lipids (phospholipids); Carbohydrates	[23], [26], [46], [47]
≈ 1398	C=O symmetric stretching of COO^- group, C-O symmetric stretching*; C-O bending (carboxylate ions)*; CH_3 and $N^+(CH_3)_3$ symmetric bending*	Proteins and carbohydrates; Mixed region (carboxylic groups); Membrane lipids (phospholipids)	[23], [45]–[47]
≈ 1338	CH_2 wagging*	Membrane lipids (phospholipids)	[45], [47]
≈ 1320	C-O stretching	Carbohydrates	[23]
≈ 1290	N-H bending in plane, C-N stretching*; C-O stretching; N-H thymine/cytosine deformation	Proteins (amide III); Carbohydrates; Nucleic acids	[23], [26], [44], [45]
≈ 1242	N-H bending in plane, C-N stretching*; P=O asymmetric stretching of PO_2^- group	Proteins (amide III, mainly α-helix conformation); Phosphodiester groups of nucleic acids	[26], [44], [45]
≈ 1168	Ester and CO-O-C antisymmetric stretching*; C-O, C-C stretching and C-O-H, C-O-C deformation*	Membrane lipids (phospholipids); Carbohydrates	[44], [45], [47]
≈ 1115	C-O, C-C stretching, C-O-H, C-O-C deformation and C-O-C asymmetric stretching*;	Carbohydrates; Phosphodiesters, RNA	[23], [26], [44]

	P-O-C symmetric stretching, C-O stretching of C-OH group		
≈ 1077	C-O, C-C stretching, C-O-H, C-O-C deformation and C-O-C asymmetric stretching*; PO_2^-, CO-O-C symmetric stretching*;	Carbohydrates; Membrane lipids (phospholipids) and nucleic acids sugar backbone	[23], [26], [44], [47]
≈ 1032	C-O, C-C stretching, C-O-H, C-O-C deformation*; C-O symmetric stretching	Carbohydrates; Nucleic acids sugar backbone	[23], [26], [44]
≈ 987	C-O, C-C stretching, C-O-H, C-O-C deformation, C-H bending*; CH_3-N asymmetric stretching	Carbohydrates; Membrane lipids (phospholipids)	[23], [44]
≈ 924	C-O, C-C stretching, C-O-H, C-O-C deformation*; $N^+(CH_3)_3$ symmetric stretching*	Carbohydrates; Membrane lipids (phospholipids)	[44], [47]

*Characteristic band assignments of biological samples (not specific for plasma)

**Not characteristic of biological samples

7. CONCLUDING REMARKS

Regarding the handling of some biofluids, such as blood, challenges remain to overcome. One of these challenges is the development of a reliable, standardized and marketable test for assessing the AD blood biomarkers. It is necessary that this test can be applied into standard clinical practise; whereat definitive clinical trials are needed to define their true diagnostic value [21,51].

A particular attractive item in focus in the last decade is combination of different spectroscopic techniques, such as FTIR and FT-Raman, for analysis of complex biological samples (e.g. body fluids and tissues). This arise the challenge of computer-based pattern recognition techniques elaboration, capable of providing effective data reduction and optimal classification results, from spectral data of samples collected in all IR regions. Possible candidates for this kind of data process/analysis pass through modern neural network (ANN) analysis strategies and effective optimal-feature extraction algorithms [29]. In the future it will be also necessary to apply FTIR and/or FT-Raman in samples of different stages of dementia, such the case of AD, to confirm if the spectra changes along disease progression. It could be also helpful compare the results of neuroimaging techniques and the spectra data. [35]

Recently, an immunologic ATR-FTIR sensor was used to study the secondary structure change of the Aβ peptide to β-sheet in early stages of AD, this can be helpful in the diagnosis of the disease. This ATR sensor removed Aβ peptide out of fluids (e.g. blood or CSF), and FTIR was subsequently applied to analyse Aβ secondary structure [33]. A new door opened for the application of vibrational spectroscopic techniques in dementia research, namely at discovering new, non-invasive and reliable biomarkers.

Finally, since diagnosis of multifactorial dementias cannot rely on a unique marker, the use of a combination of different biomarkers is of extremely importance. In addition, comparison of metabolic and proteomic profiles within the same disease and between different forms of dementia can significantly, increase the specificity of the new biomarkers, thus contributing to a more accurate and differential diagnosis. [52, 53]

8. AIMS OF THE STUDY

The main objectives of the present work are:

- Confirm some hypotheses of previous studies by FTIR;
- Identify the main metabolic characteristics present in obtained FTIR spectra;
- Discriminate samples in groups (e.g. control vs AD) through data multivariate analysis and confirm the location of the samples on the scores diagram;
- Identify the more significant altered metabolites and their eventual role at the disease context.

Chapter 2

1. INFRARED SPECTROSCOPY

Infrared spectroscopy is a technique based on the vibrations of the atoms of a molecule that can be very useful because can give information about the purity of a compound and about its structure. In the electromagnetic spectrum there are several radiation regions, the radiation visible to the human eye, radiowave, microwave, infrared, ultraviolet, X-ray and γ-ray. Infrared radiation is used in infrared spectroscopy and is a kind of radiation that is absorbed by different materials. In the electromagnetic spectrum the infrared is localized between the visible and microwave regions. The basic principle of this technique is when an organic molecule is exposed to infrared radiation the radiant energy matches the energy of a specific molecular vibration, absorption occurs. A plot that shows the absorption of infrared radiation against the wavelength of infrared radiation is called infrared spectrum. The instrument used to obtain the infrared spectrum is IR spectrometer and the way that is obtained is: the infrared radiation pass through the sample and then the fraction of the incident radiation that is absorbed at a particular energy is determined, which will result in the identification (qualitative analysis) of the materials. The peaks of energy observed in the absorption spectrum correspond to the frequency of a vibration of a part of a molecule of the sample and their size give information about the amount of material present. The only material from which it is not possible to observe an infrared spectrum is metal and the sample can be in any state solid, liquid or gaseous, what is an advantage because it allows the utilization of infrared spectroscopy in different areas. Some substances that absorb infrared radiation are powder, glass, crystals, solutions, pastes, films, liquids, fibres and vapours. The areas that use this technique most are materials science, life science and surface science and the samples are in the majority in the solid or liquid state. [51-55]

The major difference between the visible absorption spectra and the infrared absorption spectra is that in the first spectra (visible) it is only possible to observe one or two broad bands and in the second (infrared) it is possible to see many and quite sharp bands, for example organic compounds have a considerable number of infrared absorption bands. The cause of this difference is that the infrared absorptions are due to vibrational sates of atoms in a molecule, so infrared spectrum is a vibrational spectrum and the motions of atoms in the molecule are named molecular vibrations; in contrast the visible absorption spectrum is an electronic spectrum because it is related to the states of electrons in a molecule. [51]

In an infrared spectrum the ordinate axis matches to the absorption intensity and the abscissa axis matches to the wavelength but there is a particularity in the mid-infrared region, sometimes it is used the wavenumber as an alternative to wavelength in the abscissa axis. The wavenumber is the inverse of wavelength and is the number of light waves per unit length, the units in which is expressed are cm^{-1}. In the case of near-infrared region the wavelength is frequently used as the abscissa axis when the near-infrared spectrum is measured as an extension of a visible absorption spectrum. [51, 55]

The spectral measurements and the spectrum are made with the aim of determine a signal, the signal is the quantity of radiation absorbed, reflected or emitted by the sample, the signal is generally represented by S. But when someone obtains a signal it also obtains a noise that can come from different sources, the noise can be represented by a N. In a spectrum is also possible to rate it quality, for that it is necessary to determine the signal-to-noise ratio (S/N ratio, SN ratio or SNR) of the bands; the quality of the spectrum is higher when the signal-to-noise ratio is higher. [51]

Molecules have molecular vibrations and molecular rotations that are discreet energy levels of electronic motions. When molecules absorb energy they suffer a transition from a lower energy state to a higher energy state, for example when a molecule is irradiated by electromagnetic waves which may diverge from ultraviolet light to microwaves it occur a transition. But the transition has to fulfil some conditions such as:

- "The energy of a photon should coincide with the energy difference between an energy level of the molecule (usually the ground-state level) and a higher energy level (an excited-state level)." [51, 55]

There are also other rule called selection rule that are based in quantum mechanics and group theory and these rule say that to occur infrared absorption the molecule must have a specific aspect: an electric dipole moment of the molecule must change during the vibration, so there are "infrared-active" molecules (i.e. heteronuclear diatomic molecule) and "infrared-inactive" molecules (i.e. homonuclear diatomic molecule). In the case of infrared-active molecules the dipole moment of a molecule changes as the bond expands and contracts in contrast in the infrared-inactive molecules its dipole moment remains zero no matter how long the bond. [51, 53, 55]

Transitions between the energy levels of molecular vibrations are what lead to infrared absorptions mostly. Then it is possible to say that the vibrational spectra are constituted by infrared absorption spectra, Raman spectra and neutron inelastic scattering spectra. [51]

There are "pure" vibrational spectra that is an infrared spectra observed from liquids and solids because in these kind of samples free rotation of molecules does not occur. On the contrary the infrared absorption spectra observed from gases are vibration-rotation spectra because in that spectrum it is possible to detect some fine structures that are result of the transitions associated with rotational energy levels. [51]

Infrared radiation is absorbed by the molecule when the dipole moment of a molecule is changed due to a molecular vibration, and the radiation absorbed has the same frequency as the molecular vibration, due that this process of infrared absorption happen by electric interaction of molecules with infrared radiation. The absorption of infrared radiation by the molecule leads to the transition of it from the v=0 (ground vibrational state) to v=1 (first excited vibrational state) and this process is named the fundamental tone. Although less likely to happen the transition could be from v=0 to

v=2,3,4…, in these cases it is called overtones but the intensity of these absorptions are weaker than in the first case. If the transitions are between excited vibrational states it is denominated hot bands, but usually they are not seen. [51]

1.1. Types of infrared radiation

The infrared radiation can be divided into three types depending on the wavelength: near, mid and far infrared radiation. It is commonly defined the wavelength of 0.78 μm to 3 μm (12820 – 4000 cm^{-1}) for near-infrared region; 3 μm to 30 μm (4000 – 400 cm^{-1}) for mid-infrared region; and 30 μm to 300 μm (400 – 33 cm^{-1}) for far-infrared region. [51, 52, 53, 55]

1.1.1. *Near-infrared region*

In the near-infrared region it is observed the overtones or combinations of the fundamental stretching bands which occur in the 3000–1700 cm^{-1} region and the bands involved are result of C–H, N–H or O–H stretching. In this region the intensity of the bands is generally weak. [53]

1.1.2. *Mid-infrared region*

The mid-infrared region is the region that usually can give more information and it may be identified four different regions: the X–H stretching region (4000–2500 cm^{-1}), the triple-bond region (2500–2000 cm^{-1}), the double-bond region (2000–1500 cm^{-1}) and the fingerprint region (1500–600 cm^{-1}). O–H, C–H and N–H stretching are responsible for the fundamental vibrations in the region of 4000-2500 cm-1; the triple-bond absorptions are due to the high force constants of the bonds such as C≡C bonds or C≡N bonds; in the third region (2000-1500 cm^{-1}) the C=C and C=O stretching lead to the principal bands. The 1500-600 cm^{-1} region is called the “fingerprint region” because some vibrations may vary by hundreds of wavenumbers and it is what happens in this region where small steric or electronic effects in the molecule lead to large shifts, so the majority of the bands are not assigned and the spectrum works as a “fingerprint” of the molecule. [53]

1.1.3. *Far-infrared region*

The far-infrared region can give some information about the vibrations of molecules containing heavy atoms, molecular skeleton vibrations, molecular torsions and crystal lattice vibrations. Crystal lattice vibrations are result of the movement of whole molecular chains with respect to each other in crystalline solids; the molecular torsions occur because the rotation about single bonds is not “free”, so when certain small groups are bonded to a large group, they undergo a motion with respect to the heavier “anchor” group; bending modes are usually no more than one-half of the wavenumber of the corresponding stretching mode, thereby in far-infrared region skeletal bending modes involving an entire molecule occur for molecules containing heavier atoms; in the case of the vibrations involving heavy atoms they can be useful for characterizing compounds containing halogen atoms, organometallic compounds and inorganic compounds. [53]

2. MOLECULAR VIBRATIONS

When a molecule interacts with infrared radiation changes in molecular dipoles associated with vibrations and rotations occur. The larger this change, then the more intense will be the absorption band. The energy of a molecule in a specific moment is the result of the sum of the following energy terms, electronic energy, vibrational energy, rotational energy and translational energy. Electronic energy is associated with the energy transitions of electrons as they are distributed throughout the molecule, either localized within specific bonds, or delocalized over structures, such as an aromatic ring. Vibrational energy is linked to the absorption of energy by a molecule as the component atoms vibrate about the mean center of their chemical bonds. Rotational energy is defined as the tumbling motion of a molecule, which is due to the absorption of energy within the microwave region. Translational energy is associated to the displacement of molecules in space as a function of the normal thermal motions of matter. [53, 55, 56]

Diatomic molecules have two degrees of rotational freedom, three degrees of translational freedom and one of vibrational freedom. The atoms of polyatomic molecules have 3 degrees of freedom, which correspond to the Cartesian coordinates (x, y, z) of each atom in the molecule. There are two types of triatomic molecules: linear and non-linear. Non-linear molecules have 3 rotational and 3 translational degrees of freedom, the remaining (3n-6) correspond to fundamental vibrations. Linear molecules have 2 degrees of rotational freedom and 3 of translational freedom, therefore in this situation the remaining fundamental vibrations are 3n-5. [52, 53]

In a molecule the bond length of the atoms can vary or they can move out of its present plane, it corresponds to stretching (axial deformation - Change in inter-atomic distance along bond axis) and bending (angular deformation - Change in angle between two bonds), that are collectively referred as vibrations. There are two different types of stretching, symmetric stretching and asymmetric stretching *(figure 3)*. About bending it is possible to distinguish four different types, rocking, scissoring, wagging and twisting *(figure 4)*. [52, 53, 55, 57]

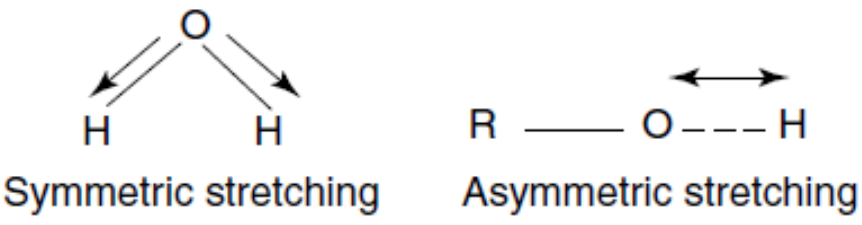

Figure 3| Symmetric and asymmetric stretching vibrations. [53]

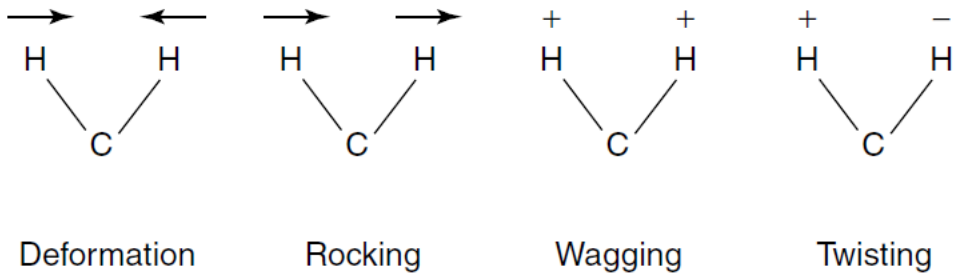

Figure 4| Different types of bending vibrations. [53]

Diatomic molecules have only one mode of vibration, a stretching motion. A linear polyatomic molecule has four modes, two of which have the same frequency and non-linear polyatomic molecules have three modes, one is due to a bending motion and the other two correspond to stretching motions. [53]

It is not possible to isolate the motion of two atoms in a molecule from the motion of the rest of the atoms in the molecule. One atom can be shared by two oscillating bonds and when this happens it is said that the vibrations of the two bonds are coupled. The result is that if one bond contracts, the other bond will contract or expand, depending if is an asymmetrical or symmetrical stretching. In coupling, in place of superimposed bands as expected, are observed bands at different frequencies. There are some factors that can influence coupling: in stretching vibrations coupling occurs when there is a common atom between two vibrating bonds; bending vibrations coupling occurs if there is a common bond between vibrating groups; if coupling is between a stretching vibration and a bending vibration occurs if the stretching bond is one side of an angle varied by bending vibration; if coupled groups have roughly equal energies the coupling is greatest; there is no coupling between groups separated by two or more bonds. [52, 57]

3. COMPLICATING FACTORS

There are some factors that can influence and difficult the analyses of an infrared spectrum, called complicating factors, sometimes they can lead to important changes to the spectra and may result in the misinterpretation of bands, some of them are:

3.1. Overtone and combination bands:

Combination bands are the result of the absorption of energy simultaneously for two bands absorbing at v1 and v2. Overtone bands are analogous and are multiples of the fundamental absorption frequency. The energy necessary for the first overtone is the double of the energy required in the fundamental and the first overtone will appear in the

spectrum at twice the wavenumber of the fundamental because the energy is proportional to the frequency absorbed and this is proportional to the wavenumber *(figure 5)*. [53]

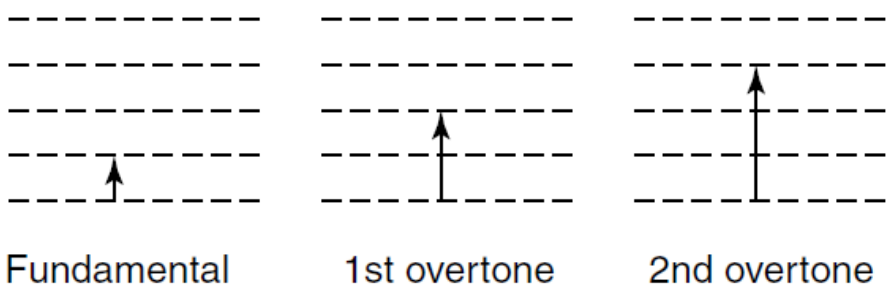

Figure 5| Energy levels for fundamental and overtone infrared bands. [53]

3.2. Fermi Resonance:

Sometimes it is possible that two bands appear in the place where only one is supposed to appear, for example when an overtone or a combination band has the same frequency as, or a similar frequency to, a fundamental. This is the Fermi resonance effect and it is stronger when the frequencies match. [53]

3.3. Coupling:

Vibrations in the skeletons of molecules become coupled and that vibrations involve a large part of the carbon backbone and oxygen or nitrogen atoms. The result is the same number of vibrational modes, but at different frequencies, and bands can no more be ascribed to one bond. Coupling is more likely to occur in C–C stretching, C–O stretching, C–N stretching, C–H rocking and C–H wagging motions. [53]

3.4. Vibration-Rotation bands:

Like explained before the gaseous heteronuclear molecules have a specific spectrum and to examine the length of one bond it is necessary to separate the lines that appear in the spectrum. [53]

4. FOURIER TRANSFORM INFRARED SPECTROSCOPY

One type of infrared spectroscopy is FTIR that is a global, sensitive, and highly reproducible physicochemical analytical technique that identifies structural moieties of biomolecules on the basis of their IR absorption. FTIR can help to identify unknown

materials, can determine the quality or consistency of a sample and can determine the amount of components in a mixture. Some advantages of FTIR are:

- The measurements obtained with this technique are very accurate and reproducible;
- It is a very reliable technique for positive identification of virtually any sample;
- It is very sensitive allowing the identification of even the smallest of contaminants then can be used for quality control or quality assurance;
- The sensitivity and accuracy of the detectors and a wide variety of software algorithms increased the practical use of infrared for quantitative analysis. [54, 58]

4.1. Fourier-Transform Infrared Spectrometers

In the past, since the 1940s were used dispersive instruments to obtain infrared spectra, nowadays the spectrometers used are the Fourier-transform infrared spectrometers (Michelson Interferometers are the most used) which enhanced the acquisition of infrared spectra. Some advantages of instruments used currently over the older instruments are:

- Is a non-destructive technique;
- Provides a precise measurement method which requires no external calibration; these instruments employ a HeNe laser as an internal wavelength calibration standard so they are self-calibrating - Connes Advantage;
- Can increase speed, collecting a scan every second because all of the frequencies are measured simultaneously - Felgett Advantage;
- Sensitivity can be improved: the detectors are much more sensitive and the optical throughput is much higher which results in much lower noise levels - Jacquinot Advantage;
- Fast scans enable the co-addition of several scans in order to reduce the random measurement noise to any desired level - signal averaging;
- Is mechanically simple with only one moving part, the moving mirror in the interferometer is the only continuously moving part in the instrument. [54]

The principal components of a Fourier-transform Infrared Spectrometers *(figure 6)* are the source, the interferometer, the sample, the detector, the amplifier, the analog-to-digital converter and a computer. [53, 54]

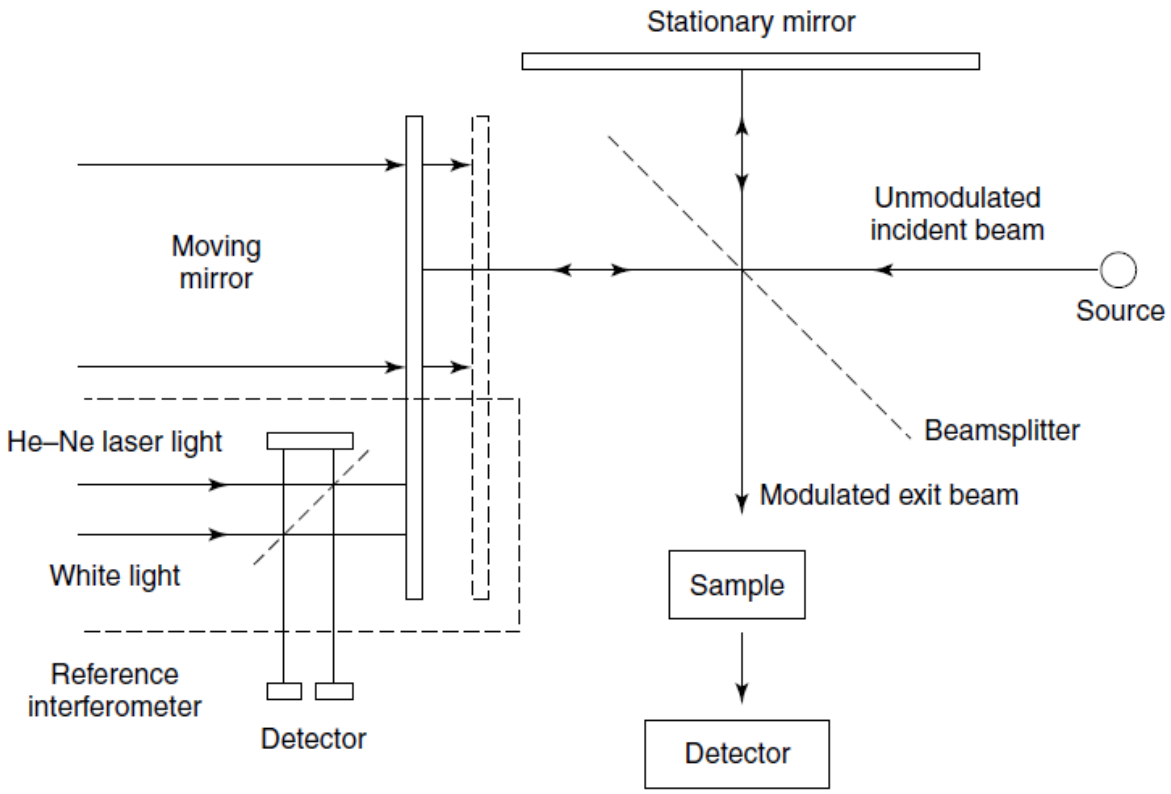

Figure 6| Schematic representation of a Michelson interferometer, showing the principal components. [53]

The first step of a FTIR analysis is the infrared energy is emitted from the source, and the beam passes through an aperture which controls the amount of energy presented to the sample and after to the detector. The source used in FTIR spectrometers depends on the region that it will be examined. For near-infrared region the source used is tungsten-halogen lamps; for the mid-infrared region the source used is a Globar or Nernst source; for the far-infrared region it is necessary to use a high-pressure mercury lamp. [53, 54]

After that the beam enters the interferometer where the “spectral encoding” takes place. Michelson interferometers are composed of two perpendicularly plane mirrors, one of which can travel in a direction perpendicular to the plane, one is a flat mirror which is fixed in place, the other is a flat mirror which is on a mechanism which allows this mirror to move a very short distance (typically a few millimetres) away from the beamsplitter. The beamsplitter is a semi-reflecting film that bisects the planes of the two mirrors. According to the region that is necessary analyse, mid-, near-, or far-infrared region the material used in the beamsplitter is different. For the mid- or near-infrared regions some of the materials used are germanium or iron oxide coated onto an ‘infrared-transparent’ substrate such as potassium bromide or caesium iodide. In the far-infrared region the materials used are thin organic films like poly (ethylene terephthalate). When an accurately parallel beam of monochromatic radiation passed into an ideal beamsplitter

50% of the incident radiation will be reflected to one of the mirrors and the other 50% will be transmitted to the other mirror. After that the two beams are reflected and return to the beamsplitter to recombine and interfere. The beamsplitter transmit 50% of the beam reflected from the fixed mirror and the remaining 50% is reflected back in the direction of the source. The beam that will be detected in FTIR spectrometry is called the transmitted beam and emerges from the interferometer at 90° to the input beam. [53, 54]

When evaluating an infrared spectrum there are several factors related with the moving mirror that is need to be considered, for example it has to be accurately aligned and must be capable of scanning two distances so that the path difference corresponds to a known value. The transformation of the digitized information on the interferogram into a spectrum can lead also to some errors because the transformation carried out in practice involves an integration stage over a finite displacement rather than over an infinite displacement and the mathematical process of Fourier transformation assumes infinite boundaries. Another source of error arises if the sample intervals are not exactly the same on each side of the maxima corresponding to zero path differences. [53]

Posteriorly the transmitted beam enters the sample compartment, where can be transmitted through or reflected off of the surface of the sample. It is here where the sample will absorb specific frequencies of energy that are unique of that sample. [53, 54]

The subsequent step is the passage of the beam to the detector for final measurement. It is not only the source that it is different according to the region, the detectors used in FTIR spectrometers is also different from region to region. To analyse a near-infrared region it is used lead sulphide photoconductors detectors; for the mid-infrared region two types of detectors can be used, the most common is a pyroelectric device incorporating tryglycine sulphate (DTGS) in a temperature-resistant alkali halide window and if it is needed a more sensitive analysis the detector used is a mercury cadmium telluride (MCT) cooled to liquid nitrogen temperatures; for far-infrared region the detectors used are, germanium or indium–antimony detectors, operating at liquid helium temperatures. [53, 54]

Finally the measured signal is digitized and sent to the computer where the Fourier transformation takes place to obtain the infrared spectrum. Computer has a number of functions in the modern infrared instruments. Some of those functions are:

- Controls the instrument: it sets scan speeds and scanning limits, and starts and stops scanning;
- It reads spectra into the computer memory from the instrument as the spectrum is scanned;
- Spectra may be manipulated using the computer: by adding and subtracting spectra or expanding areas of the spectrum of interest;
- Scan the spectra continuously and average or add the result in the computer memory;
- Plot the spectra. [53, 54]

When a FTIR analysis is done is also necessary to measure a background spectrum, which is a measurement with no sample in the beam and one background measurement can be used for many samples. This measurement is needed because there needs to be a relative scale for the absorption intensity and then is compared to the measurement with the sample in the beam to determine the "percent transmittance". This allows detecting the spectral features strictly due to the sample. [53, 54]

4.2. ATR (Attenuated Total Reflectance Spectroscopy)

ATR (Attenuated Total Reflectance spectroscopy) is a technique that utilizes the phenomenon of total internal reflection. A beam of radiation entering a crystal will undergo total internal reflection when the angle of incidence at the interface between the sample and crystal is greater than the critical angle, where the latter is a function of the refractive indices of the two surfaces. The beam penetrates a fraction of a wavelength beyond the reflecting surface. The beam will lose energy at the wavelength where the material absorbs when a material that selectively absorbs radiation is in close contact with the reflecting surface. The resultant attenuated radiation is measured and plotted as a function of wavelength by the spectrometer and gives rise to the absorption spectral characteristics of the sample. The depth of penetration in ATR spectroscopy is a function of the wavelength, λ, the refractive index of the crystal, n_2, and the angle of incident radiation, θ. The depth of penetration of the evanescent wave into the sample is a function of the crystal material and the angle of incidence. Deeper penetration is achieved with either a smaller incidence angle or a lower refractive index crystal. The depth of penetration also increases with the wavelength. [53, 59]

The most common material used in the crystals used in ATR cells are zinc selenide (ZnSe), germanium (Ge) and thallium–iodide (KRS-5) because those are materials that have low solubility in water and are of a very high refractive index. Zinc Selenide is a relatively low cost ATR crystal material and is ideal for analysing liquids and non-abrasive pastes and gels but it is not particularly robust with a working pH range of 5-9. Germanium has a much better working pH range and can be used to analyse weak acids and alkalis. Germanium has by far the highest refractive index of all the ATR materials available which means that the effective depth of penetration is approximately 1 micron. Although having a higher cost, diamond is the best ATR crystal material because of its robustness and durability. Diamond can be used to analyse a range of samples from single particles and fibbers to corrosive liquids. [53, 59, 60]

There are different designs of ATR cells which allow the analysis of liquid and solid samples. It is possible monitor the spectral changes for the continuous flow of solutions through the cell with time because it is possible to set up a flow-through ATR cell by including an inlet and outlet in the apparatus. [53]

Some of the advantages of ATR are:

- Faster sampling;

- Improving sample-to-sample reproducibility;
- Minimizing user to user spectral variation;
- Better quality database building for more precise material verification and identification. [60]

5. MID-INFRARED SPECTROSCOPY APPLIED IN BIOLOGICAL SAMPLES

Human plasma and serum are commonly used matrices in biological and clinical studies. Plasma and serum are derived from full blood the difference is the process to obtain them; to obtain plasma is necessary to add an anticoagulant such as EDTA (Ethylenediamine tetraacetic acid) or heparin before the removal of blood cells. For serum it is necessary the coagulation of the blood and after that the process of centrifugation leads to the release of proteins and metabolites into the serum by the platelets. One study showed that reproducibility was significantly better for plasma than for serum which may result from the less complicated collecting procedure for plasma, as it does not require time to coagulate. In terms of metabolite concentrations it was observed to be higher in serum and the sensitivity is also higher in the serum. [61]

Serum or plasma infrared spectroscopy analyses are very useful in diagnosing and monitoring a great diversity of disorders. If the concentrations are high enough MIR spectra can distinct these six organic species, glucose, total protein, albumin, triglycerides, urea and cholesterol. The MIR region gives a “fingerprint” characteristic of molecular species, like mentioned before is the region that gives more information. In plasma FTIR spectrum it is possible to observe the peaks associated to its constituents because each biomolecule have its own structure and it will exhibit a unique FTIR spectrum with more or less specific absorption peaks. To determine the absorption spectra of some biomolecules it is necessary to subtract the absorption spectra of others, one example is the case of lactate; to see the absorption pattern of lactate it is necessary to subtract the absorption attributable to glucose first. [58, 62]

A study that compared the results of 35 plasma FTIR spectra revealed that albumin was the biomolecule present in the highest concentration in plasma; albumin represents 65% of plasma proteins and 45% of the total plasma mass. [58]

One problem of IR spectroscopy is that water is the most abundant species found in all biological fluids, and that can interfere with the IR spectra. [62]

Chapter 3

1. METHODS OF STUDY

1.1. Study group

According to previous works the inclusion criteria for the present study group were: age between 50-90 years, resident in Aveiro region, with complaints including objective memory impairment or other cognitive complains. In contrast the excluding criteria contain individuals undergoing chemotherapy or radiotherapy, suffering from psychiatric illness (e.g. bipolar disease, schizophrenia), or using illicit drugs. [63, 64]

Sample collection and cognitive evaluation of individuals was carried out at several centres for primary health care from Aveiro region.

The project was approved by the ethics committee of the Regional Health Centre - Coimbra, protocol number 012 804 of April 4, 2012.

The cognitive tests applied to the study group were: Clinical Dementia Rating scale (CDR), Mini-Mental State Examination (MMSE) and Geriatric Depression Scale (GDS).

In this study cognitive dysfunction was considered when CDR ≥ 0.5. The CDR scale is:

- 0: normal function;
- 0.5: transition level (questionable dementia);
- 1.0: significant loss (almost always a clear correlation with dementia);
- 2.0: loss of moderate cognitive function;
- 3.0: severe loss.

MMSE is a test that allows patient stratification according to the education level:

- Cutoff of 22 for 0-2 years schoolarship;
- 24 for 3-6 years;
- 27 for more than 7 years.

The GDS scale is a test with 15 questions that allowed exclusion from the study of depressed individuals.

According to cognitive evaluation, 45 individuals were subdivided in 3 groups: the age and sex matched control group, presenting negative result for all the 3 cognitive tests; the putative AD group, with a positive result for CDR and MMSE scales but negative for GDS and other neuropathologies; the other neuropathologies group, which includes subjects suffering from other pathologies or mixed disorder and thus also positive on CDR and MMSE scales. It was also reunited other clinical data related to presence of some AD risk factors, namely the manifestation of comorbidities such as DM, dyslipidaemia or hypertension (HTN). Samples identification is in table 4.

Table 4| Characterization of study samples group according to sex, age and cognitive evaluation.

COD	Sex	Age	MMSE	CDR	Condition
C1J	F	65	-	-	Control
C2J	F	81	-	-	Control
C3J	F	78	-	-	Control
C4J	F	65	-	-	Control
C5J	F	72	-	-	Control
C6J	F	72	-	-	Control
C7J	F	78	-	-	Control
C8J	F	73	-	-	Control
C9J	M	82	-	-	Control
C10J	F	81	-	-	Control
C11J	M	74	-	-	Control
C12J	F	49	-	-	Control
C13J	F	75	-	-	Control
C14J	F	84	-	-	Control
C15J	F	75	-	-	Control
C16J	M	78	-	-	Control
C17J	F	75	-	-	Control
C18J	F	72	-	-	Control
C19J	F	77	-	-	Control
C20J	F	75	-	-	Control
C21J	M	81	-	-	Control
C22J	M	82	-	-	Control
C23J	F	80	-	-	Control
C24J	F	79	-	-	Control
C25J	F	72	-	-	Control
D1J	M	80	+	-	Putative AD
D2J	F	65	+	-	Putative AD
D3J	F	84	+	+	Putative AD
D4J	F	74	+	+	Putative AD
D5J	F	49	+	+	Putative AD
D6J	M	83	+	+	Putative AD
D7J	F	74	+	+	Putative AD
D8J	F	72	+	+	Putative AD
D9J	M	74	+	+	Putative AD
D10J	F	78	+	+	Putative AD
D11J	F	85	+	+	Putative AD
D12J	F	78	+	+	Putative AD
D13J	F	76	+	+	Putative AD
D14J	F	82	+	+	Putative AD
D15J	F	86	+	+	Putative AD
D16J	M	80	+	-	Putative AD
D17J	F	88	+	+	Putative AD
D18J	F	80	+	+	Putative AD
D19J	F	76	+	+	Other/mixed dementia
D20J	F	76	+	+	Other/mixed dementia

1.2. Analysis conditions

To the present study it was necessary to make some optimization in the method. The optimization in the sample collection, in the FTIR spectral acquisition and with a drying process was according to previous works, “Identification of Alzheimer biomarkers by FTIR – a pilot study” and” Identification of potential Alzheimer’s disease biomarkers in plasma using FTIR”. [63, 64]

To obtain the plasma aliquots of the samples, it was used it was used tubes K2 EDTA 5 mL with gel separator and then it was applied a centrifugal force of 1800g during 15 minutes at 8ºC. After this process the blood cells were separated from plasma. The plasma aliquots performed were of 30 µL and they were stored at -80 ºC. In this work the spectrometer used to acquire the spectra was Perkin-Elmer Spectrum BX FT-IR™. The spectra were obtained in a range of 4000-600 cm^{-1}, at resolution of 8 cm^{-1}, with 64 co-added scans. For each sample 8 µL of plasma were used. 16 spectra were acquired, that corresponds to 40 minutes, which is the estimate drying time. During all the process the room temperature and humidity were maintened at ± 23ºC and ± 39%, respectively.

This work it is a continuation of two previous works, [63] and [64]. Like mentioned before, with this work it is intended to confirm some hypotheses of those previous studies and to confirm the location of the samples on the scores diagram (reproducibility). For that spectra of 3 samples existing in larger quantities were repeated and their location in scores diagram were compared with the location of spectra acquired previously.

Three spectral regions were analysed, 3500-2700 cm^{-1}, 1800-1400 cm^{-1} and 1200-900 cm^{-1}. 16 spectra were obtained for each sample and in the previous works has been used only the last 3 in the analysis. In this work it was used only the last two since it was observed that the spectrum 14 still had water. As can be observed in figure 7 the spectra are different under the 900 cm^{-1} region which, indicating that they have different amounts of water. The region under 900 cm^{-1} is not used in multivariate spectra analysis but the presence of water also affects different spectral regions and can therefore affect the results. The multivariate analysis was repeated with this reduced data-set.

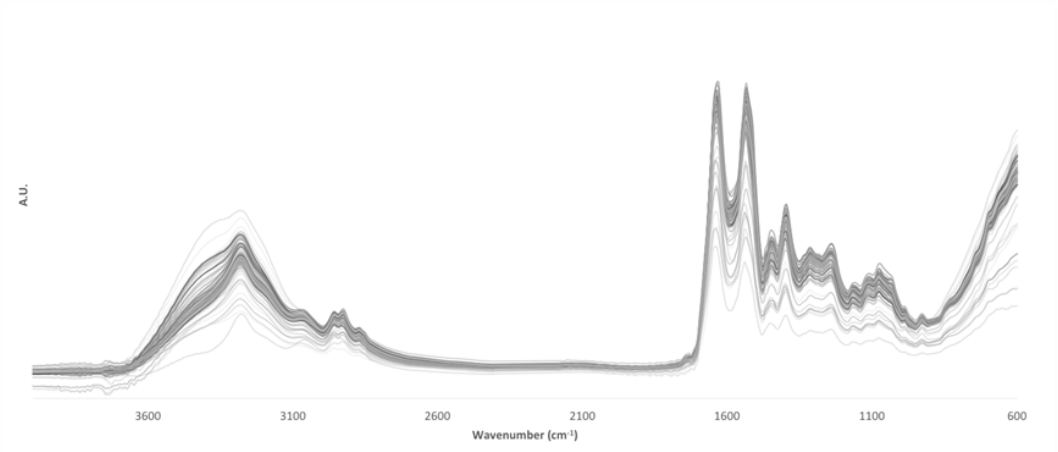

Figure 7| All 14 spectrum, showing that it still had water

1.3. Main MIR regions of interest for study aims

It is possible to divide the MIR region in other smaller spectral regions where strong absorption bands can be associated to specific components (figure 8). Those regions are: fatty acids region; amide region, ascribed primarily to proteins and peptides; mixed region, ascribed to carboxylic groups of proteins, free amino acids and polysaccharides; and the polysaccharide region. Besides, there are others spectral regions such as the one that is relevant to RNA, DNA and phospholipid content. [76]

The 900-600 cm^{-1} region can be called the "true fingerprint region" because it shows a range of weak but extremely characteristic features. Some bands that can be observed in this region are bands arising from aromatic ring vibrations of phenylalanine, tyrosine, tryptophan, and the various nucleotides. [77]

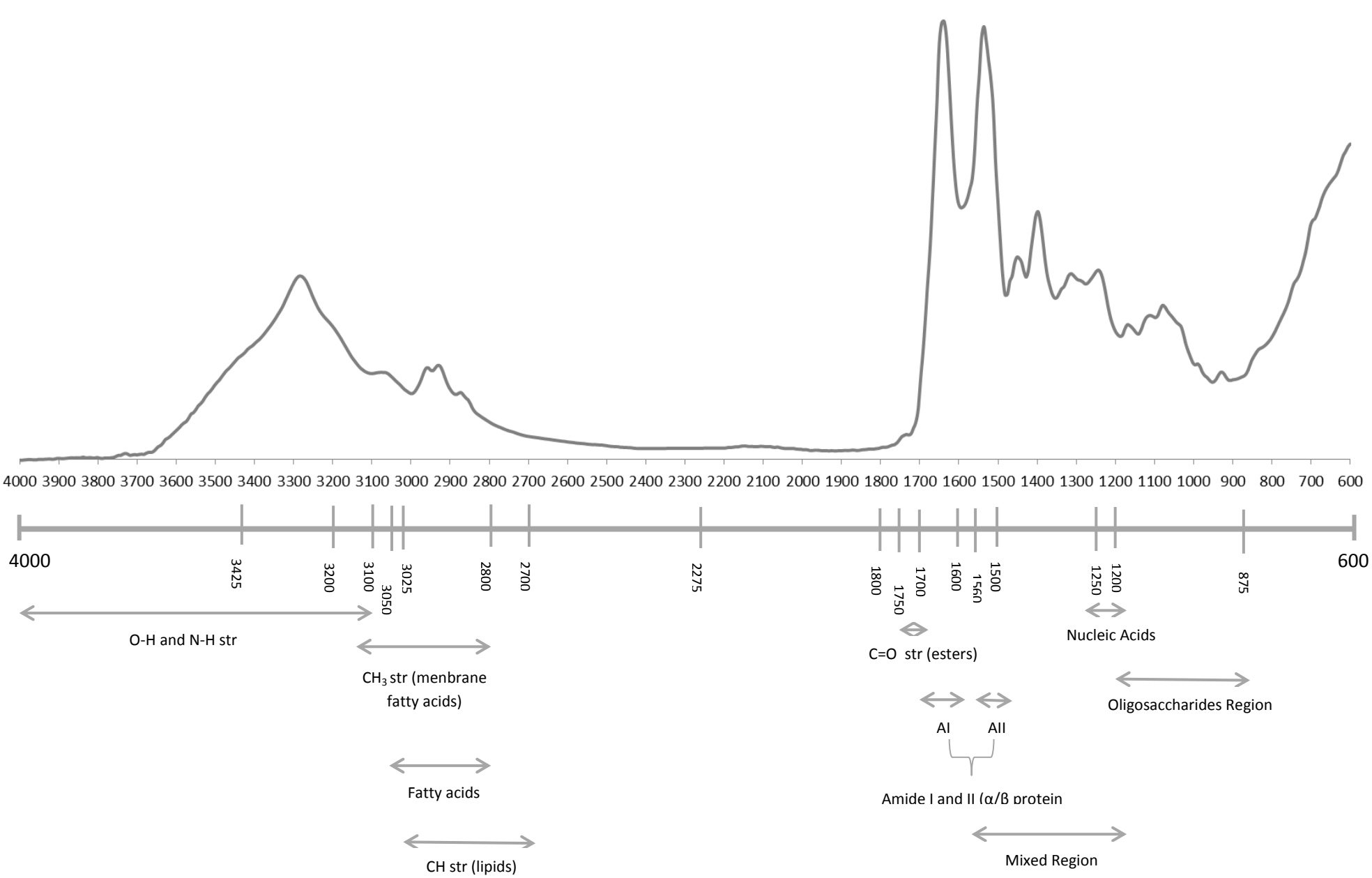

Figure 8| FTIR example spectra with main regions of FTIR spectra in a range of 4000-600 cm^{-1}.

2. RESULTS AND DISCUSSION

2.1. Localization of the new samples

In this study three samples were repeated, and new spectra of those samples were acquired. After that, the spectra were joined to the previous "data set" and new multivariate analyses were made. The following images (figure 9-14) are related to results obtained by comparing the location of samples that were repeated in this study with the ones of the previous studies. It is possible to see that their location is very similar, the new spectra are very close to the previous ones.

With these results it is possible to say that the results of multivariate analysis are reliable and that the classification models are robust. The results also showed that the frozen samples at -80 ° C didn´t suffer significant changes.

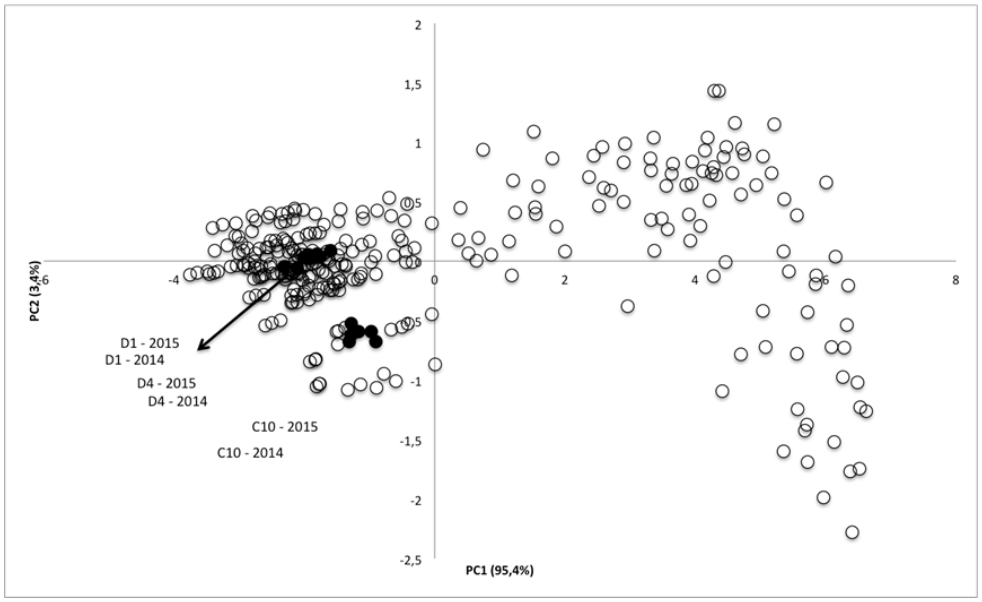

Figure 9| PCA scores scatter plot of 3500-2700 cm^{-1} spectral region showing the location of the repeated samples

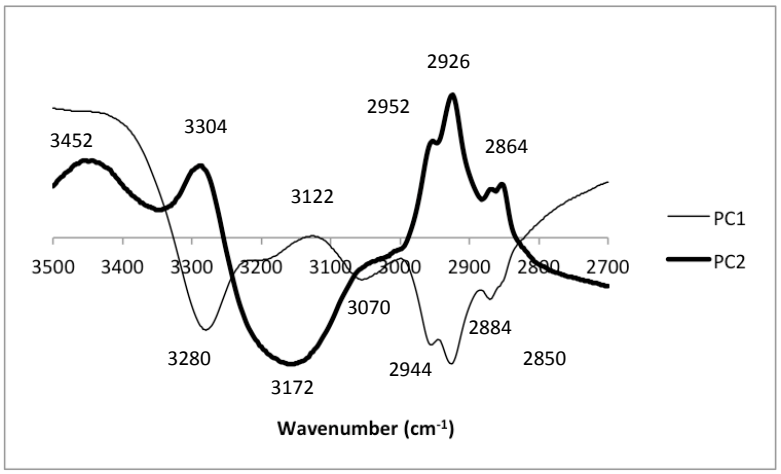

Figure 10| PCA loadings of 3500-2700 cm^{-1} spectral region

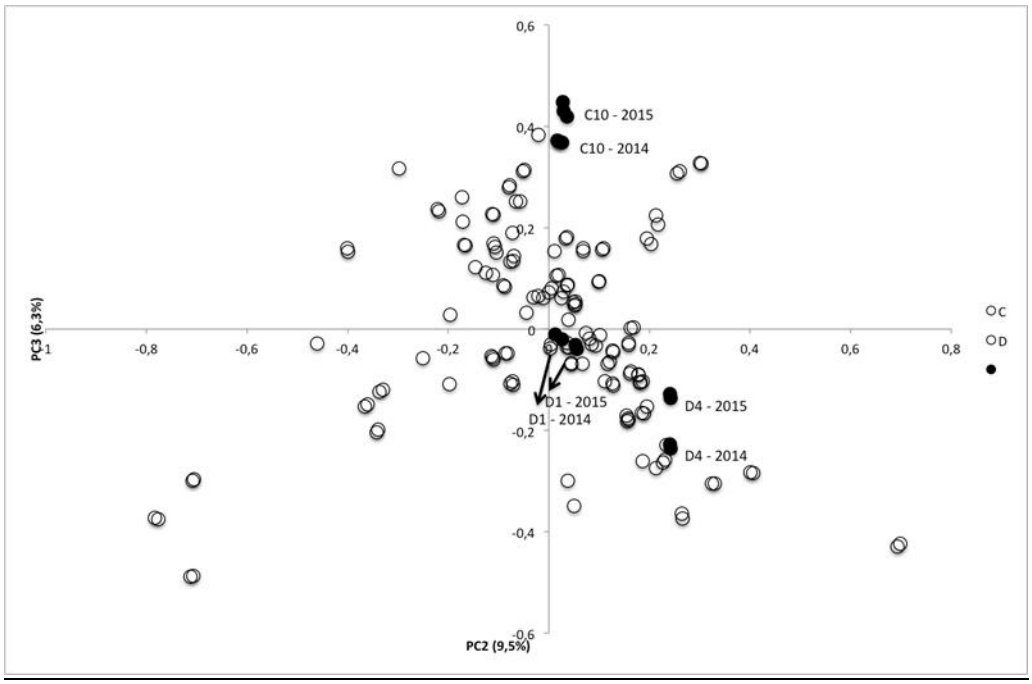

Figure 11| PCA scores scatter plot of 1800-1400 cm^{-1} spectral region showing the location of the repeated samples

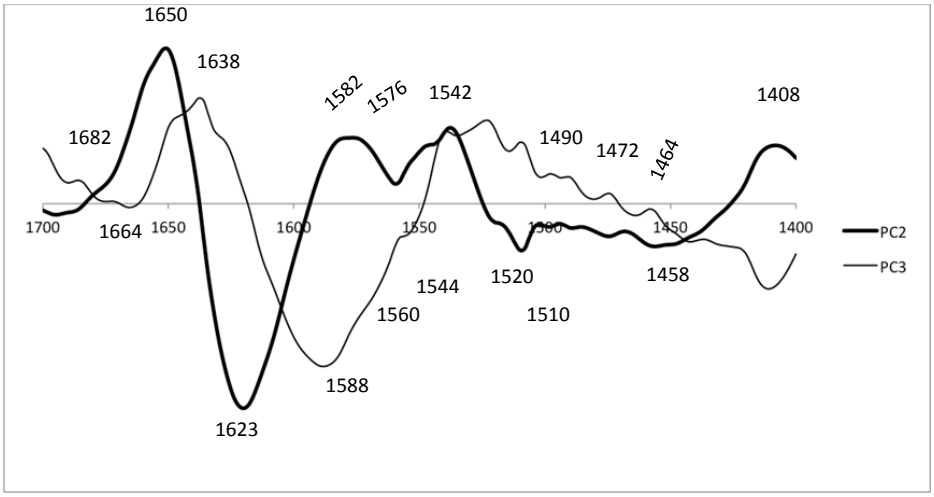

Figure 12| PCA loadings of 1800-1400 cm^{-1} spectral region

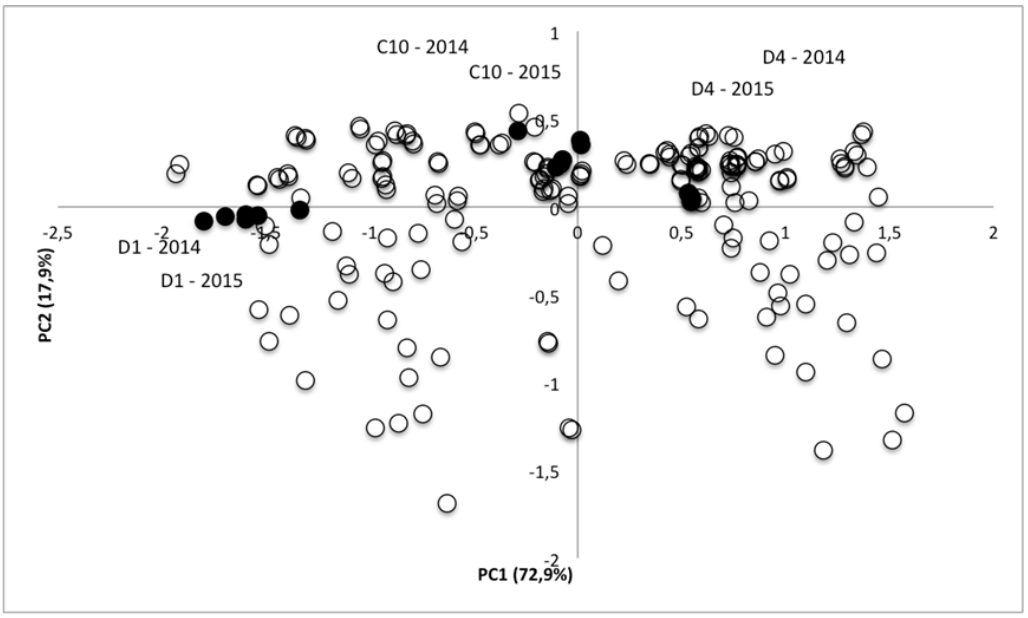

Figure 13| PCA scores scatter plot of 1200-900 cm^{-1} spectral region showing the location of the repeated samples

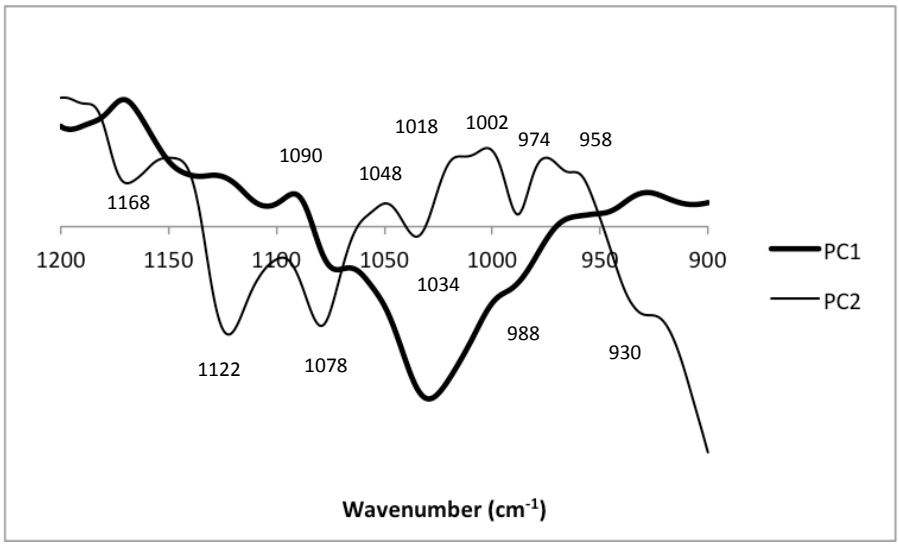

Figure 14| PCA loadings of 1200-900 cm^{-1} spectral region

2.2. Spectral analysis

The obtained spectra were analyzed to identify the maximum wavenumber peaks at both control and disease samples. Each of these spectral signals have one or more assignment (specific type of molecular vibration), that corresponds to a certain chemical group or a chemical family of compounds. This will help in the identification of the main chemical components of the plasma samples (table 5).

Table 5| Spectral assignments of plasma and serum samples.

Peaks (cm^{-1})	Assignments	Plasma contents	Ref.
≈ 3718	O-H stretching and an intermolecular vibration of CO_2 and phenol**	Presence of gaseous CO_2	[42]
≈ 3454	N-H stretching	Proteins (amide A)	[43]
≈ 3286	N-H stretching, H-O-H symmetric and asymmetric stretching*	Proteins (amide A)	[44], [45]
≈3282	N-H stretching	Proteins (amide A)	[65], [66]
≈ 3190	N-H symmetric stretching	mainly cis-ordered sub-structures	[26]
≈3088	N-H stretching	Proteins (amide B)	[65], [66]
≈ 3052	N-H stretching	Proteins (amide B)	[26]
≈2966	C-H asymmetric stretching of CH_3 group	Lipids (cholesterol esters, triglycerides)	[67], [68], [69]
≈ 2962	C-H asymmetric stretching of CH_3 group*	Lipid acyl chains in lipid bilayers (phospholipids)	[29], [44], [46], [47]
≈2944	C-H asymmetric stretching of CH_2 group	Lipids (long chain fatty acids, phospholipids)	[67], [68], [69]
≈ 2938	C-H stretching of CH_2 and CH_3 group*	Fatty acids	[29], [43], [44]
≈ 2878	C-H symmetric stretching of CH_3 group*	Lipid acyl chains in lipid bilayers (phospholipids)	[29], [44], [46], [47]
≈2872	C-H symmetric stretching of CH_3 group	Lipids (long chain fatty acids, phospholipids)	[67], [68], [69]
≈1750	C=O symmetric stretching	Lipids (cholesterol esters, triglycerides)	[67], [68]
≈ 1740	C=O stretching	Fatty acid esters (triglycerides), lipid bilayers (phospholipids)	[23], [44], [46]
≈ 1716	C=O stretching	Carbonic acid, phospholipid sub-structures, purine bases from nucleic acids	[23], [29], [44], [48]
≈ 1638	C=O stretching*; NH_3^+ asymmetric in plane bending (rocking)*	Proteins (amide I for β-sheet); Membrane lipids (phospholipids)	[29], [44], [47], [49]
≈ 1636	C=O stretching and N-H in plane bending	Proteins (amide I)	[70], [71]
≈ 1536	N-H bending in plane, C-N stretching*	Proteins (amide II)	[29], [44], [45]
≈ 1516	N-H in plane bending and C-H stretching	Proteins (amide II)	[70], [71]
≈ 1512	CC (phenyl ring) stretching, CH in plane bending*	tyrosine band (proteins side chain)	[29], [44], [50]
≈ 1474	C-H asymmetric bending of CH_2 group / C-H bending of CH_2 group	Lipids (fatty acids, phospholipids, triglycerides)	[67], [68], [69]
≈ 1470	CH_2 bending; C-H asymmetric bending;	Proteins; Carbohydrates;	[23], [26], [29], [47]

	CH_2 symmetric in plane bending (scissoring)*	Lipid acyl chains in lipid bilayers (phospholipids)	
≈ 1454	C-H asymmetric bending of CH_2 group / C-H bending of CH_2 group	Lipids (fatty acids, phospholipids, triglycerides)	[67], [68], [69]
≈ 1452	CH_2 bending and CH_3 asymmetric in plane bending (rocking)*; C-O symmetric stretching	Proteins, membrane lipids (phospholipids); Carbohydrates	[23], [26], [46], [47]
≈ 1402	COO stretching	Amino acids side chains	[67], [72]
≈ 1398	C=O symmetric stretching of COO^- group, C-O symmetric stretching*; C-O bending (carboxylate ions)*; CH_3 and $N^+(CH_3)_3$ symmetric bending*	Proteins and carbohydrates; Mixed region (carboxylic groups); Membrane lipids (phospholipids)	[23], [45]–[47]
≈ 1342	CH_2 wagging***	Collagen	[73], [74], [75]
≈ 1338	CH_2 wagging*	Membrane lipids (phospholipids)	[45], [47]
≈ 1320	C-O stretching	Carbohydrates	[23]
≈ 1301	N-H bending and C-N stretching	Proteins (amide III)	[70], [71]
≈ 1290	N-H bending in plane, C-N stretching*; C-O stretching; N-H thymine/cytosine deformation	Proteins (amide III); Carbohydrates; Nucleic acids	[23], [26], [44], [45]
≈ 1246	N-H bending and C-N stretching	Proteins (amide III)	[70], [71]
≈ 1242	N-H bending in plane, C-N stretching*; P=O asymmetric stretching of PO_2^- group	Proteins (amide III, mainly α-helix conformation); Phosphodiester groups of nucleic acids	[26], [44], [45]
≈ 1168	Ester and CO-O-C antisymmetric stretching*; C-O, C-C stretching and C-O-H, C-O-C deformation*	Membrane lipids (phospholipids); Carbohydrates	[44], [45], [47]
≈ 1115	C-O, C-C stretching, C-O-H, C-O-C deformation and C-O-C asymmetric stretching*; P-O-C symmetric stretching, C-O stretching of C-OH group	Carbohydrates; Phosphodiesters, RNA	[23], [26], [44]
≈ 1077	C-O, C-C stretching, C-O-H, C-O-C deformation and C-O-C asymmetric stretching*; PO_2^-, CO-O-C symmetric stretching*;	Carbohydrates; Membrane lipids (phospholipids) and nucleic acids sugar backbone	[23], [26], [44], [47]
≈ 1032	C-O, C-C stretching, C-O-H, C-O-C deformation*; C-O symmetric stretching	Carbohydrates; Nucleic acids sugar backbone	[23], [26], [44]
≈ 994	C-O ribose, C-C***	Ribose	[73], [74], [75]
≈ 987	C-O, C-C stretching, C-O-H, C-O-C deformation, C-H bending*; CH_3-N asymmetric stretching	Carbohydrates; Membrane lipids (phospholipids)	[23], [44]
≈ 924	C-O, C-C stretching, C-O-H, C-O-C deformation*; $N^+(CH_3)_3$ symmetric stretching*	Carbohydrates; Membrane lipids (phospholipids)	[44], [47]

*Characteristic band assignments of biological samples (not specific for plasma)

**Not characteristic of biological samples

***Only present in plasma

The spectral band at 3718 cm^{-1} might be related to a higher level of plasma acidity, which is usually found at perturbations of acid/base blood balance mechanisms that in turn might be associated to presence of general oxidative stress responses. In acidic conditions such as brain ischemia and hypoxia, I2 PP2A (inhibitor-2 of protein phosphatase-2A) is cleaved into a C-terminal and an N-terminal fragments that are known to bind to PP2A (protein phosphatase-2A) catalytic subunit inhibiting its activity. Once, that a decrease in PP2A can be a cause of the protein tau abnormal hyperphosphorylation in AD, it might be possible the involvement of brain acidosis in AD pathogenesis. [78]

The peptide bond could exhibit nine characteristic IR-active amide bands (A, B and I-VII). Nonetheless, at the present study only amide A, B and I-III were identified in FTIR spectrum. The N-H stretching vibration gives rise to the amide A band between 3310 and 3270 cm^{-1}, it is exclusively localized on the NH group and is therefore insensitive to the conformation of polypeptide backbone. The amide A band is usually part of a Fermi resonance doublet with the second component absorbing weakly between 3100 and 3030 cm^{-1} (amide B). Amides I and II, as mentioned below (2.2.2), are the major bands in the protein FTIR spectrum, with amide I providing the most insight into secondary structure. Amides III and IV are very complex bands resulting from mixtures of several coordinate displacements. Out-of-plane motions could be found in amides V, VI and VII. Given the technical and theoretical limitations, only amide bands I, II and III are used for analysis of protein secondary structure. [43, 45]

It is believed that in neurodegenerative disorders there is significant lipid damage in brain tissues. In FTIR spectrum, lipids have characteristic C-H stretching vibrations between 3025 and 2700 cm^{-1}. For $–CH_2$ functional group, the asymmetric and symmetric C-H stretching vibrations are found at ≈2920 and 2850 cm^{-1}, respectively and for $-CH_3$ functional groups are found at ≈ 2957 and 2872 cm^{-1}, respectively. In addition, unsaturated olefinic C=C-H stretching vibration has a unique vibrational frequency of 3012 cm^{-1}. [48, 79]

The presence of a carbonyl group in a compound can be identified by the strong IR band at the region 1650-1850 cm^{-1}, which corresponds to the C=O stretching vibration. At the present study, FTIR spectra analysis reveals some peaks in this region (1740, 1716 and 1638 cm^{-1}), which might be related to lipid hyperoxidation, especially 1740 cm^{-1} band. Indeed, the 1638 cm^{-1} band corresponds to β-sheet of amide I, which can be related to conformational changes of protein α-helices. [80]

Tyrosine is a relative strong infrared absorber due to its polar character and the ring mode near 1517 cm^{-1} is one of its most intensive bands. [50]

In relation to nucleic acid biochemistry, in a FTIR spectra the most characteristic findings are the C=O stretching vibrations from the purine (1717 cm^{-1}) and pyrimidine (1666 cm^{-1}) bases, besides antisymmetric (1224 cm^{-1}) and symmetric (1087 cm^{-1}) PO_2-stretching vibrations at the 1500-1000 cm^{-1} region. [48]

In AD there are also some changes in the tertiary structure at the 780-739 cm^{-1} spectral range. [35]

The next step was to apply a method of multivariate analysis for all 45 samples in the four different spectral regions 3500-2700 cm^{-1}, 1800-1400 cm^{-1} and 1200-900 cm^{-1}. The presented results correspond to the multivariate analysis obtained without the 14 replicate, that, as mentioned before, presents high amount of water.

2.3. PCA analysis and identification of main sample groups

It was possible to cluster the samples in some sub-groups, within control and putative AD groups, through the analysis of the scores and loadings obtained by PCA methodology.

2.3.1. *Spectral range of 3500-2700 cm^{-1}*

In this spectral range (figure 15) it is possible to observe the presence of lipids (e.g. saturated or unsaturated), especially fatty acids and phospholipids, and its implications for cognitive health and dementia states. Besides, some information of amide A and B regions of proteins could be found in this range.

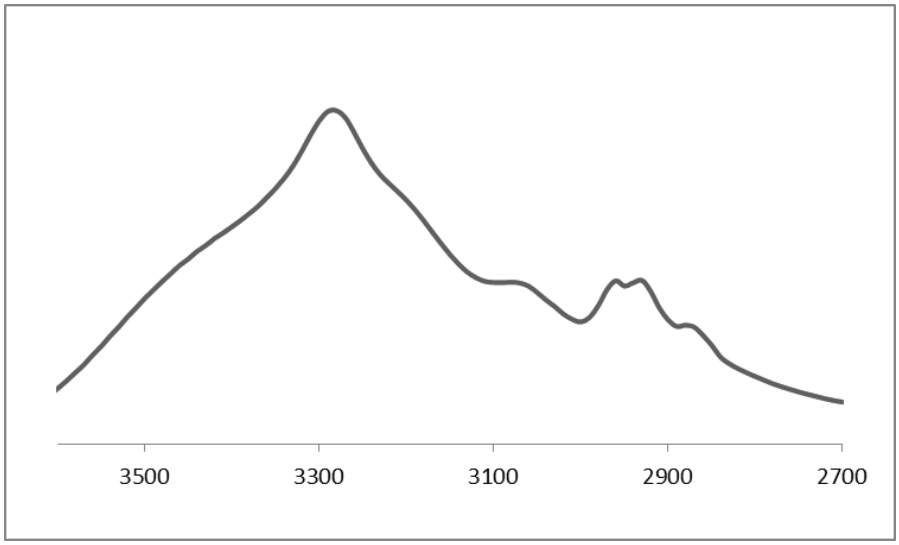

Figure 15| Representative spectral region of 3500-2700 cm^{-1}

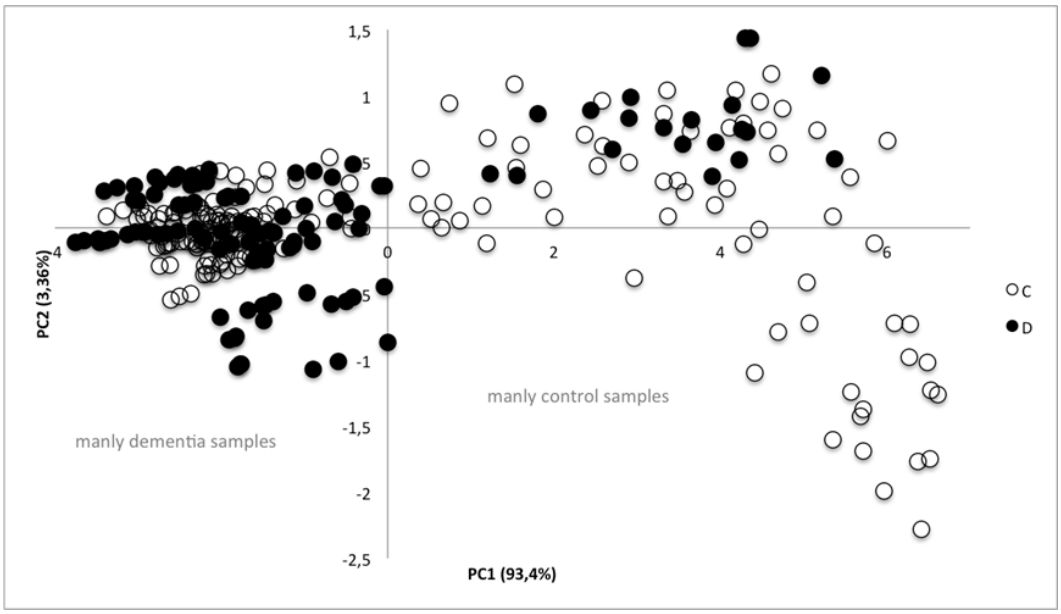

Figure 16| PCA scores scatter plot of 3500-2700 cm^{-1} spectral region showing PC1 *vs.* PC2. C: control samples; D: dementia/cognitive impairment samples

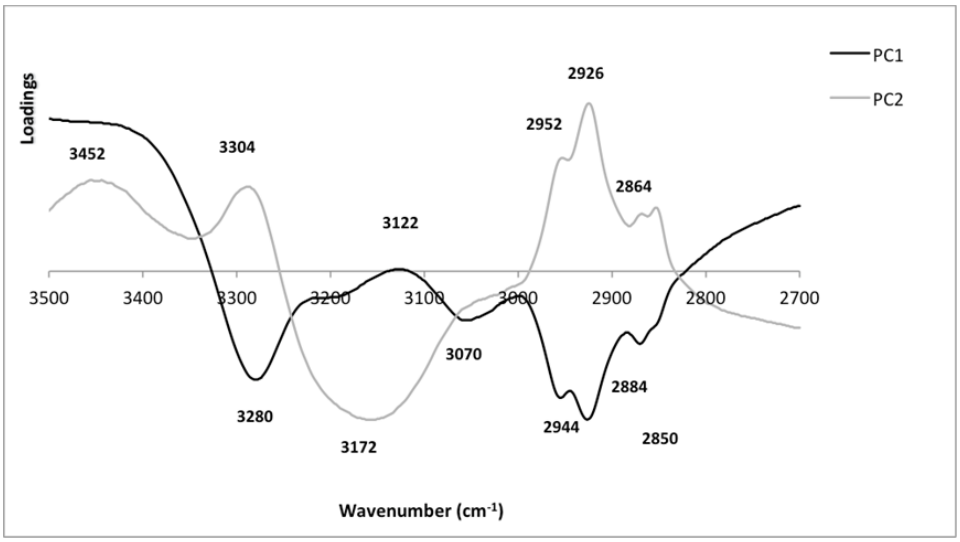

Figure 17| PCA loadings of 3500-2700 cm^{-1} spectral region showing the main maximum wavenumber peaks.

Figure 16 shows that is possible to discriminate control samples that the great part of them are located in PC1. However disease samples are present in all quadrants, but mainly concentrated in negative PC1 region.

Indeed, PCA loadings (figure 17) analysis turns possible to divide disease samples into two distinct groups, according to the presence of different kinds of molecular alterations (Table 6). Besides, disease samples present at positive PC1 express a more disperse distribution among control samples group.

There are some factors that can influence the results, such as: the presence of comorbidities, disorder of mixed nature, medication, or even factors as age or sex of the subjects.

Table 6| Assignments of the main maximum peaks from PCA loadings (range of 3500-2700 cm^{-1}).

Peak (cm^{-1})	PCs	Assignment
3400	PC1 (+)	N-H stretching of amide A
3286	PC1 (-) PC2 (+)	N-H stretching of amide A
3172	PC1 (-) PC2 (-)	O-H stretching band of carboxylic acids
3070		N-H stretching of amide B
3026		N-H stretching of amide B
2952	PC1 (-) PC2 (+)	C-H asymmetric stretching of -CH_3 (fatty acids)
2926		C-H asymmetric stretching of -CH_2 (fatty acids)
2884		C-H asymmetric stretching of -CH_2 (membrane lipids)
2864		C-H symmetric stretching of -CH_3 (membrane fatty acids)
2850		C-H symmetric stretching of -CH_2 (membrane fatty acids)

The spectral region between 4000-3100 cm^{-1} can give information resulting from O-H stretching modes (≈3400 cm^{-1}) and from N-H stretching vibrations (amide A and amide B) and the region between 3100 and 2800 cm^{-1} gives information resulting from C-H stretching vibrations of $–CH_3$ and $–CH_2$ functional groups. [29]

In the region with mainly disease samples it wasn´t detected any peak close to 3012 cm^{-1}, which could indicate very low content of unsaturated lipids. These results corroborate the fact that significant low levels of PUFAs in brain tissue are usually related to AD condition. [48, 79]

In the region between 3025-2800 cm^{-1} it was possible to identify several peaks such as 2952 cm^{-1}, 2926 cm^{-1}, 2884 cm^{-1}, 2864 cm^{-1} and 2850 cm^{-1}, associated with the presence of saturated lipids. Alterations in this spectral range, mainly CH_2 stretching vibrations, can indicate changes in the lipid order of the biological system. A high content of saturated lipids is related to some vascular perturbations that are strong correlated with higher risk of dementia development. [47, 48, 53, 80]

Due to these results it can be said that there is an unbalance between the content of saturated and unsaturated lipids, favoring the first one.

It was also seen a strong band at 3172 cm^{-1} that is related to strong O-H stretching vibrations, which is an evidence that it is essentially characterized by carboxylic acids. The presence of carboxylic compounds can be related with protein structural and functional disturbances in the neurodegeneration process and with changes in protein conformation, which will lead to a different localization of amide B region. [48, 53, 80, 81]

The PC1 positive region is composed mainly of control samples it can be seen also some dispersed disease samples inside its frontiers. The region with mainly control samples is characterized by the presence of assignment for amide A related to the peak 3400 cm^{-1}. [45]

The fact of some controls are at negative PC1 indicates that these samples could present similar biochemical pattern to the disease samples. This means that those controls could have a higher risk of developing dementia or it can show the presence of cognitive impairment in a pre-clinical stage.

2.3.2. *Spectral range of 1800-1400 cm^{-1}*

The spectral range 1800-1400 cm^{-1} (figure 18) is mainly related to protein conformation mode trough analysis of protein secondary structure (amide I and II) but also to chemical properties of nucleic acids bases, fatty acids and carbohydrates.

Figure 18| Representative spectral region of 1800-1400 cm^{-1}

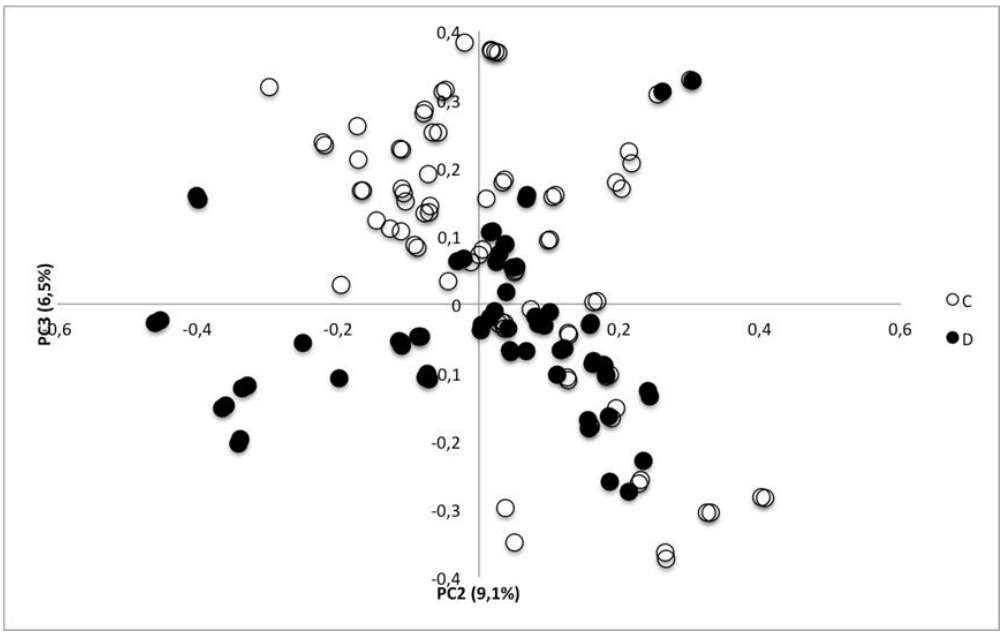

Figure 19| PCA scores scatter plot of 1800-1400 cm^{-1} spectral region showing PC2 vs. PC3. C: control samples; D: dementia/cognitive impairment samples.

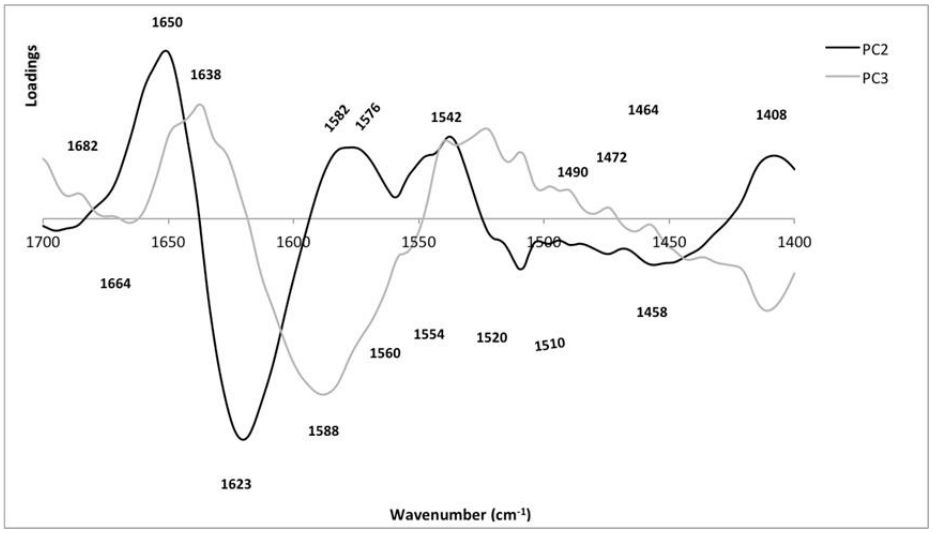

Figure 20| PCA loadings of 1800-1400 cm^{-1} spectral region showing the main maximum wavenumber peaks.

According to figure 19 is possible to say that the majority of dementia subjects have negative PC3 value and the control samples have mainly positive PC3, though there are also some controls in Q4. The main maximum peaks from PCA loadings are present in table 7.

Table 7| Assignments of the main maximum peaks from PCA loadings (range of 1800-1400 cm^{-1}).

Peak (cm^{-1})	PCs	Assignments
1682	PC3 (+)	C=O guanine deformation N-H in plane; unordered random coils, turns and loops (amide I)
1664	PC2 (+)	C=O band of α-helical structure (amide I)*, turns and loops
1650	PC2 (+)	C=O symmetric stretching band of α-helical structure (amide I)
1638	PC3 (+)	C=O stretching band of parallel β-sheet (amide I)
1623	PC3 (+)	C=O stretching band of parallel β-sheet (amide I)
1588	PC3 (-)	N-H bending in plane and C-N stretching (amide II); benzene ring vibrations from arginine
1582	PC3 (-)	C=N imidazole ring stretching (nucleic acids); benzene ring vibrations from arginine
1576	PC3 (-)	N-H bending in plane and C-N stretching (amide II); NH_3^+ symmetric bending (membrane lipids); C=N imidazole ring stretching (nucleic acids)
1560	PC2 (+)	N-H bending in plane and C-N stretching of amino acids (amide II); CO_2- asymmetric stretching from glutamic acid
1554	PC2 (+)	N-H deformation mode of α-helical band (amide II)*; CO2- asymmetric stretching from glutamic acid
1542	PC2 (+)	N-H bending in plane and C-N stretching of amino acids (amide II)
1520	PC2 (-) PC3 (+)	N-H bending in plane and C-N stretching of amino acids (amide II);
1510	PC2 (-) PC3 (+)	N-H bending in plane and C-N stretching of amino acids (amide II); C-H in plane bending of phenyl rings (tyrosine)
1490	PC2 (-) PC3 (+)	$N_+(CH_3)_3$ asymmetric bending (membrane lipids)
1472	PC2 (-) PC3 (+)	CH_2 scissoring of proteins and CH_3 scissoring of phospholipids (membrane lipids)
1464	PC3 (-)	CH_2 scissoring and CH_3 scissoring and asymmetric bending of phospholipids (membrane lipids)
1458	PC3 (-)	C=O symmetric stretching of COO^- of amino acid side chains; CH_2 bending of mainly fatty acids (membrane lipids)
1408	PC3 (-)	C=O symmetric stretching of COO^- of amino acid side chains and fatty acids; $N^+(CH_3)_3$ symmetric bending (membrane lipids)

*related to structural analysis of synthetic polypeptide

Amide I (1600-1700 cm^{-1}) and amide II (1500-1560 cm^{-1}) bands are two prominent features of a typical protein spectrum, the first is due to C=O stretching vibration and the second to the N-H bending and C-N stretching vibrations of peptide backbone. The frequency of amide I band is particularly sensitive to secondary structure what makes FTIR a valuable technique for evaluating protein aggregation at neurodegenerative disorders. [43, 48]

Two important factors in degenerative disorders are oxidative stress and free radical damage. As a result, it is not surprising that there is a decreased intensity of 1455 cm^{-1} centered peak (Table 7), which is close to the 1458 cm^{-1} peak identified at the present study (Figure 20). This results from deformation and stretching vibrations of CH_2 groups particularly in fatty acids (present in membrane lipids). [38, 48]

The 1582 cm^{-1} band might be associated to alteration of conformational state and structural stability of nucleic acid molecules. The same may also be stated for 1576 cm^{-1}, to which is added structural changes in lipids. Altered protein conformation and presence of protein aggregates typical of AD lead to different localization for amide II that can be seen in 1588 cm^{-1} peak. 1464 cm^{-1} and 1408 cm^{-1} peaks are due mainly to structural changes of associated membrane lipids, namely fatty acids and phospholipids. [44, 45, 47, 53]

Almost all of patients that belong to AD group present comorbidities, which may be translated in higher severity and faster progression of the disease condition.

In the control samples the identified 1520 cm^{-1} and 1510 cm^{-1} peaks are associated with unaltered protein conformation, without any signal that could indicate protein aggregation or presence of intermediate damaging forms like oligomers. These results are in accord with the biochemical pattern of a control sample. [43, 49]

The other peaks 1472 cm^{-1} and 1490 cm^{-1}, are associated to structural properties of membrane lipids. The 1490 cm^{-1} peak is particularly connected to membrane injury probably due to the action of oxidative stress and free radicals inductors of cell damage. The presence of some comorbidities such as DM and HTN helps the development of dementia and/or some other related neurodegenerative diseases. Once the subjects of this group suffer from those comorbidities it is possible that these subjects had already achieve the pre-MCI or initial phase of MCI state and it would be important theirs clinical monitoring.

The peaks 1682 cm^{-1}, 1638 cm^{-1}, 1623 cm^{-1} observed in control samples could be associated to the disease samples present in it, because of their coordinates and their match to amide I region of aggregated proteins (Figure 12). Indeed, 1623 cm^{-1} peak had been considered as characteristic of a protein in an aggregated state, during FTIR analysis of cerebral tissue from AD patients. [43, 48, 82]

Contrarily to fibrils, oligomers present both 1630 and 1695 cm^{-1} peaks, which correspond to an anti-parallel β-sheet conformation. In the present study 1695 cm^{-1} peak is not present loadings (Figure 13), but it doesn´t mean the complete lack of oligomer forms in the analyzed samples, and there is two peaks near to 1630 cm^{-1} (i.e. 1623 cm^{-1} and 1638 cm^{-1}), which is related to highly stable parallel β-sheet that in turn is usually associated to the presence of fibrils. A higher proportion of Aβ fibril forms is related to a later stage of the disease once it is believed that Aβ soluble oligomers are an intermediate form that precedes Aβ fibrils. The fact of the absence of 1695 cm^{-1} peak, suggested that Aβ fibrils are present in higher content than Aβ oligomers. [83]

Most of the proteins present a mixture of secondary structures, and thus, the amide I band represents a combination of these components. The 1670-1685 cm^{-1} region is related to the presence of non-β structure in protein fibrils, especially turns and loops, so, Aβ fibrils present in lower content non-β structures related mainly to 1682 cm^{-1} band. Amorphous aggregates also may present a spectral band at 1623 cm^{-1}, and they are not

associated to a higher content of β-sheet structure, contrarily to protein fibrils. The presence of a band at 1623 cm^{-1} (Figure 20), might indicate that besides protein fibrils there are also some amorphous aggregates, arising from a relatively unfolded-like partially folded and a native like conformation, respectively. [43, 48, 82]

Components of C=O band with α and β forms are related to spectral peaks at 1658 cm^{-1} and 1629 cm^{-1}, respectively, thus the 1664 and 1623 cm^{-1} peaks found in the present study are related to α and β forms. In addition, the identified peaks at 1554 and 1542 cm^{-1} that are linked to N-H deformation mode, because N-H deformation mode corresponds to a signal peak at 1550 cm^{-1}. [43]

In the other hand, control samples could be associated to signal peaks identified at 1664 cm^{-1} and 1650 cm^{-1} that are related to the typical localization of amide I of proteins mainly constituted by α-helix structures. This is corroborated by protein structural information given by 1560 cm^{-1}, 1554 cm^{-1}, 1542 cm^{-1} and 1538 cm^{-1} peaks. Nevertheless, giving the proximity of these samples to the disease ones, from both Q1 (protein aggregates) and Q4 (lipid and nucleic acids altered biochemistry), it is possible that control samples share some biochemical characteristics with disease samples. Therefore, it is quite plausible that control subjects have already been suffering with a pre-clinical form of cognitive impairment (i.e. beginning of MCI). [43, 44, 45, 84]

2.3.3. *Spectral range of 1200-900 cm^{-1}*

The spectral region 1200 - 900 cm^{-1} is usually dominated by the symmetric stretching of PO2 groups in nucleic acids and a complex sequence of peaks due mainly to strongly coupled C-C, C-O stretching and C-O-H, C-O-C deformation modes of several oligosaccharides . Besides oligosaccharides and nucleic acids structural and functional information, it is possible to identify signal peaks related to membrane lipids.

Figure 21| Representative spectral region of 1200-900 cm^{-1}

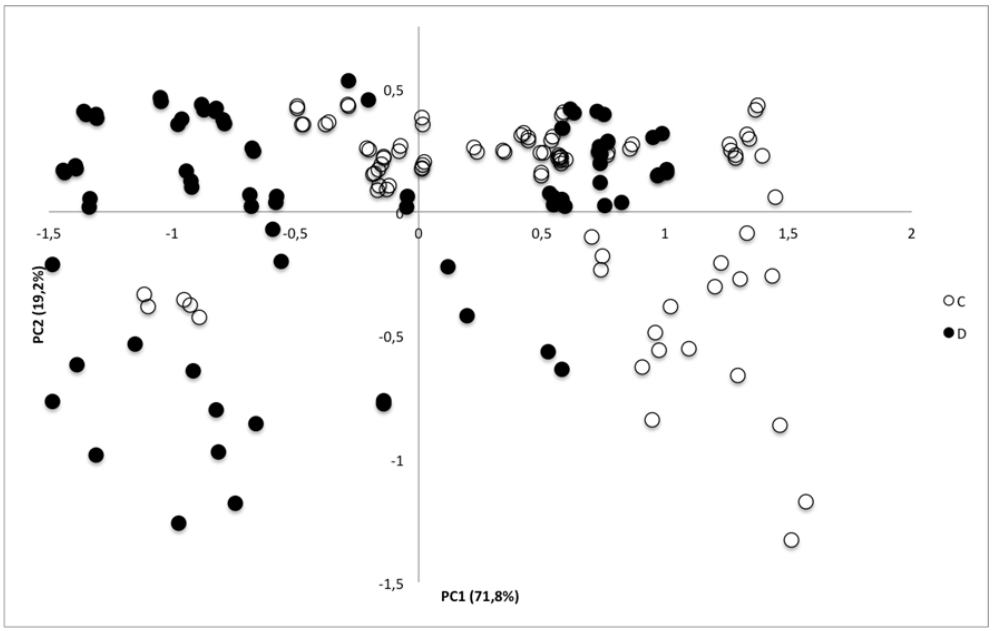

Figure 22| PCA scores scatter plot of 1200-900 cm^{-1} spectral region showing PC1 vs PC2. C: control samples; D: dementia/cognitive impairment samples

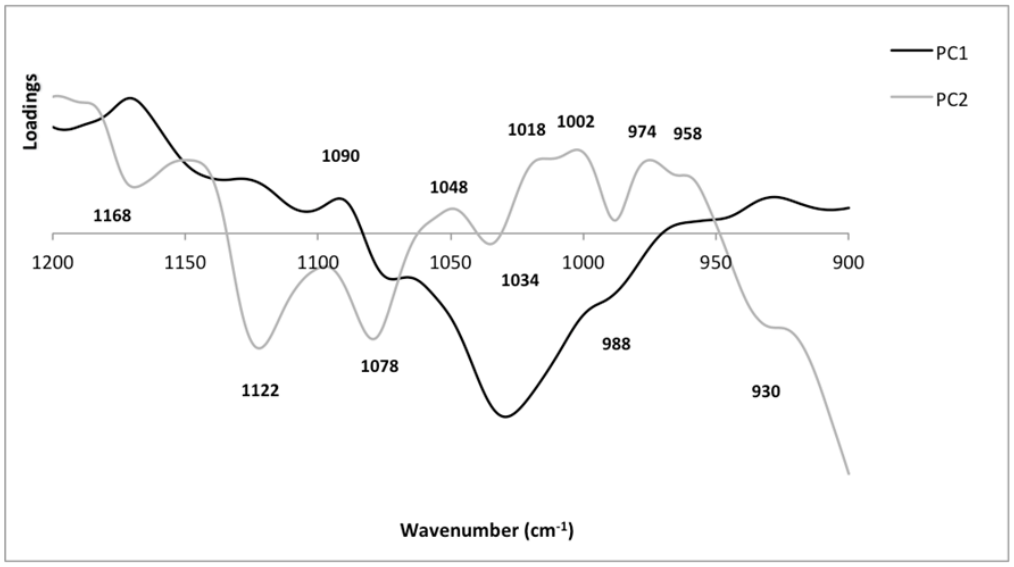

Figure 23| PCA loadings of 1200-900 cm^{-1} spectral region showing the main maximum wavenumber peaks.

The PCA scores in the figure 22 showed that is possible to identify some disease samples localized, at positive PC1 and some at negative PC1.

Table 8| Assignments of the main maximum peaks from PCA loadings (range of 1200-900 cm^{-1}).

Peak (cm^{-1})	PCs	Assignment
1168	PC1 (+)	C-O stretching of ribose from nucleic acids; CO-O-C asymmetric stretching (membrane lipids)
1122		PO stretching of phosphodiester backbone and C-O stretching of deoxyribose and ribose (nucleic acids)
1090		PO2- symmetric stretching of sugar rings (nucleic acids) and membrane lipids
1078	PC1 (-)	CO-O-C symmetric stretching (membrane lipids)
1062		Ester C-O-C symmetric stretching (phospholipids); ribose C-O stretching (nucleic acids)
1048		C-O stretching of sugar rings (nucleic acids)
1034		C-N symmetric stretching of amino acid (aliphatic amines); ribose C-O stretching (RNA)
1018		C-O stretching in osidic and protein structures; symmetric stretching of dianionic phosphate monoester (nucleic acids, especially DNA)
1002		C-O stretching in osidic and protein structures; uracil ring bending (RNA); symmetric stretching of dianionic phosphate monoester (nucleic acids, especially DNA)
988		C-O stretching in osidic and protein structures; symmetric stretching of dianionic phosphate monoester (nucleic acids, especially DNA)
974		C-O stretching in osidic and protein structures; $N^{+}(CH_3)_3$ asymmetric stretching (membrane lipids); symmetric stretching of dianionic phosphate monoester (nucleic acids, especially DNA)
958	PC1 (+)	C-O stretching in osidic and protein structures; symmetric stretching of dianionic phosphate monoester (nucleic acids, especially DNA)
930		C-O-H out of plane bending of carboxylic acids; C-O stretching in osidic and protein structures; symmetric stretching of dianionic phosphate monoester (nucleic acids, especially DNA)

The disease samples are distributed among PC1 region, having less contribute of PC2, which makes difficult to distinguish the wavenumber components of each sample. Consequently, like it is possible to see in table 8, the analysis of main maximum peaks in PCA loadings doesn´t allow differentiating clearly the biochemical pattern between the disease samples groups, once that the alterations present in both are in the majority in nucleic acids, but also in membrane lipids and proteins. It is not also possible to distinguish the control groups by PCA loadings because it has not been identified spectral bands that could be related to control characteristics.

Although it is possible to see that disease samples seems to have more contribute from negative PC1 signal peaks and on contrary the control samples presents more contribution from positive PC1 signal peaks. Which may be inferred from that information is that those two groups have contrasting biochemical characteristics, which could translate in opposing clinical profiles.

It is possible to relate the presence of hydroxyl compounds (products of lipid peroxidation and have already been reported as markers of oxidative damage in AD), with the C-O stretching bands found in the 1150-1000 cm^{-1} spectral region. In the 1200-1100 cm^{-1} region it is possible to see saturated lipids (aliphatic esters), which can lead to a higher content of saturation and consequently to a higher risk of membrane damage and vascular events. The disease individuals can have a risk of a more severe picture of neurodegeneration because the majority of them have comorbidities such as DM, HTN or dyslipidaemia and it is known that hyperoxidation of lipids, phospholipids and membranes takes place during the atherogenesis process. [53, 80, 85]

With the spectral peaks at 1122 cm^{-1}, 1090 cm^{-1}, 1048 cm^{-1}, and the ones from the 1020-930 cm^{-1} region it is possible to see that Nucleic acids molecules, especially DNA, represent a major target for free radicals when capacity of intracellular free radical scavengers and antioxidants is overcome. There are some repair enzymes systems that try to remove and replace the damaged nucleosides and repair the broken strands, but like it is possible to see by the high plasmatic levels of 8-OHdG (8-hydroxydeoxyguanosine) found in AD patient samples, the rate of DNA damage still be high. It is supposed that the accumulation of damages in DNA can contribute to progressive neuronal cell loss, since nonrepaired DNA damage can lead to programmed cell death. [38]

3. CONCLUDING REMARKS

With this work it is possible to affirm that the results obtained by FTIR and multivariate analysis are reliable and that the classification models are robust. When sample acquisition is repeated 12 months later principal components analysis (scores diagram) showed that the location of the new spectra is very close to the previous ones. Additionally the removal of all the spectra with deficient drying process (more moisture) improves results; the discrimination between putative AD and sex and age matched controls allows the identification of more defined groups. This means that some conditions, such as temperature and humidity, in the moment of the analyses will be crucial for the results and can influence them. The improvement of the discrimination between samples groups can be reflected, in the future, in the construction of robust classification models.

With the modified data set it was possible to confirm previous results. With the direct analysis of spectra it is possible to recognize the main chemical FTIR assignments in plasma, which will help in creating a pattern of chemical vibrations and identify the principal spectral regions with important information. Although that advantage, it is necessary to use multivariate data analysis techniques, such as PCA, to draw out the significant and no redundant spectra information once biological samples are very complex, and direct analysis of spectra proved to be insufficient to distinguish between the spectra of control and dementia samples.

Some IR significant regions in which are possible to acquire spectrum data with important information are 3500-2700 cm^{-1} (lipids), 1800-1400 cm^{-1} (protein conformation) and 1200-900 cm^{-1} (carbohydrates and nucleic acids structure). In the lipids region the main conclusion that is possible to take is that there is an unbalance between the content of saturated and unsaturated lipids, favouring the first one which can lead to a high potential brain damage. It could be also seen the presence of carboxylic acids that are usually related to lipid hyperoxidation, production of reactive carbonyls and protein structural and functional disturbances. In relation to the second region (protein conformation) it was found the presence of protein aggregates and the change in protein conformation for highly stable parallel β-sheet, which is usually associated to the presence of Aβ fibrils. The 1200-900 cm^{-1} region showed the presence of products of lipid peroxidation related to impairment of membranes, and nucleic acids oxidative damage.

There are some relevant clinical factors that could influence the results of this work, some of them are: the presence of several comorbidities in the majority of subjects, unknown and/or undiagnosed genetic predisposed factors, use of medication capable of affect biochemical plasma levels or the presence of a neurodegenerative disorder of mixed nature.

Finally is possible to say that FTIR analysis can be used to build classification models that in the future can be used for cognitive impairment diagnosis or identification of disease stage and prognostic evaluation, besides assessment of disease developing risk for control subjects. However it is necessary further clinical trials that enlarge the data set with fully characterized sample.

Bibliography

[1] M. Kosicek and S. Hecimovic, *"Phospholipids and Alzheimer's disease: alterations, mechanisms and potential biomarkers.,"* Int. J. Mol. Sci., vol. 14, no. 1, pp. 1310–22, Jan. 2013.

[2] C. Bazenet and S. Lovestone, *"Plasma biomarkers for Alzheimer's disease: much needed but tough to find.,"* Biomark. Med., vol. 6, no. 4, pp. 441–54, Aug. 2012.

[3] R. Arking, *The Biology of Aging: Observations & Principles,* Third edit. Oxford University Press, 2006.

[4] C. Ballard, S. Gauthier, A. Corbett, C. Brayne, D. Aarsland, and E. Jones*, "Alzheimer's disease.,"* Lancet, vol. 377, no. 9770, pp. 1019–31, Mar. 2011.

[5] P. Kumar and M. Clarck, *Kumar & Clark's Clinical Medicine*, Seventh ed. Saunders Elsevier, 2009.

[6] R. Taipa, J. Pinho, and M. Melo-Pires, *"Clinico-pathological correlations of the most common neurodegenerative dementias.,"* Front. Neurol., vol. 3, no. May, p. 68, Jan. 2012.

[7] L. Alves, A. S. a Correia, R. Miguel, P. Alegria, and P. Bugalho, *"Alzheimer's disease: a clinical practice-oriented review.,"* Front. Neurol., vol. 3, no. April, p. 63, Jan. 2012.

[8] X.-H. Xu, Y. Huang, G. Wang, and S.-D. Chen, *"Metabolomics: a novel approach to identify potential diagnostic biomarkers and pathogenesis in Alzheimer's disease.,"* Neurosci. Bull., vol. 28, no. 5, pp. 641–8, Oct. 2012.

[9] H. Hampel, R. Frank, K. Broich, S. J. Teipel, R. G. Katz, J. Hardy, K. Herholz, A. L. W. Bokde, F. Jessen, Y. C. Hoessler, W. R. Sanhai, H. Zetterberg, J. Woodcock, and K. Blennow, *"Biomarkers for Alzheimer's disease: academic, industry and regulatory perspectives.,"* Nat. Rev. Drug Discov., vol. 9, no. 7, pp. 560–74, Jul. 2010.

[10] A. El-Ansary, *"Biomarker discovery in neurological diseases: a metabolomic approach,"* Open Access J. Clin. Trials, pp. 27–41, 2009.

[11] D. I. Ellis, W. B. Dunn, J. L. Griffin, J. W. Allwood, and R. Goodacre, *"Metabolic fingerprinting as a diagnostic tool.,"* Pharmacogenomics, vol. 8, no. 9, pp. 1243–66, Sep. 2007.

[12] C. Krafft and V. Sergo, *"Biomedical applications of Raman and infrared spectroscopy to diagnose tissues,"* Spectroscopy, vol. 20, no. 5–6, pp. 195–218, 2006.

[13] F. Di Domenico, R. Coccia, D. A. Butterfield, and M. Perluigi, *"Circulating biomarkers of protein oxidation for Alzheimer disease: expectations within limits.,"* Biochim. Biophys. Acta, vol. 1814, no. 12, pp. 1785–95, Dec. 2011.

[14] S. Dong, Y. Duan, Y. Hu, and Z. Zhao, *"Advances in the pathogenesis of Alzheimer's disease: a re-evaluation of amyloid cascade hypothesis.,"* Transl. Neurodegener., vol. 1, no. 1, p. 18, Jan. 2012.

[15] R. a Sperling, P. S. Aisen, L. a Beckett, D. a Bennett, S. Craft, A. M. Fagan, T. Iwatsubo, C. R. Jack, J. Kaye, T. J. Montine, D. C. Park, E. M. Reiman, C. C. Rowe, E. Siemers, Y. Stern, K. Yaffe, M. C. Carrillo, B. Thies, M. Morrison-Bogorad, M. V Wagster, and C. H. Phelps, *"Toward*

defining the preclinical stages of Alzheimer's disease: recommendations from the National Institute on Aging-Alzheimer's Association workgroups on diagnostic guidelines for Alzheimer's disease.," Alzheimers. Dement., vol. 7, no. 3, pp. 280–92, May 2011.

[16] C. Teunissen, *"C EREBROSPINAL FLUID BIOMARKERS FOR A LZHEIMER ' S DISEASE : EMERGENCE OF THE,"* vol. 65, no. Figure 1, pp. 3–4, 2013.

[17] M. Goedert and M. G. Spillantini, *"A century of Alzheimer's disease.,"* Science, vol. 314, no. 5800, pp. 777–81, Nov. 2006.

[18] WebPat, *"The Internet Pathology Laboratory for Medical Education,"* 2014. [Online]. Available: http://library.med.utah.edu/WebPath/TUTORIAL/CNS/CNSDG004.html. [Accessed: 01-Jan-2014].

[19] L. Whiley and C. Legido-Quigley, *"Current strategies in the discovery of small-molecule biomarkers for Alzheimer's disease.,"* Bioanalysis, vol. 3, no. 10, pp. 1121–42, May 2011.

[20] R. J. Castellani, R. K. Rolston, and M. A. Smith, *"Alzheimer disease.,"* Dis. Mon., vol. 56, no. 9, pp. 484–546, Sep. 2010.

[21] A. L. Mitchell, K. B. Gajjar, G. Theophilou, F. L. Martin, and P. L. Martin-Hirsch, *"Vibrational spectroscopy of biofluids for disease screening or diagnosis: translation from the laboratory to a clinical setting.,"* J. Biophotonics, vol. 7, no. 3–4, pp. 153–65, Apr. 2014.

[22] Y. Ma, P. Zhang, Y. Yang, F. Wang, and H. Qin, *"Metabolomics in the fields of oncology: a review of recent research.,"* Mol. Biol. Rep., vol. 39, no. 7, pp. 7505–11, Jul. 2012.

[23] M. de la Guardia and S. Garrigues, Eds., *Handbook of Green Analytical Chemistry*, 1a Ed. John Wiley & Sons, Ltd, 2012.

[24] L. Wang and B. Mizaikoff, *"Application of multivariate data-analysis techniques to biomedical diagnostics based on mid-infrared spectroscopy.,"* Anal. Bioanal. Chem., vol. 391, no. 5, pp. 1641–54, Jul. 2008.

[25] R. Davis and L. J. Mauer, *"Fourier tansform infrared (FTIR) spectroscopy: A rapid tool for detection and analysis of foodborne pathogenic bacteria,"* in Current Research, Technology and Education Topics in Applied Microbiology and Microbial Biotechnology, A. Mendez-Vilas, Ed. Formatex Research Center, 2010, pp. 1582–1594.

[26] Z. Movasaghi, S. Rehman, and D. I. ur Rehman, *"Fourier Transform Infrared (FTIR) Spectroscopy of Biological Tissues,"* Appl. Spectrosc. Rev., vol. 43, no. 2, pp. 134–179, Feb. 2008.

[27] Z. Yu, G. Kastenmüller, Y. He, P. Belcredi, G. Möller, C. Prehn, J. Mendes, S. Wahl, W. Roemisch-Margl, U. Ceglarek, A. Polonikov, N. Dahmen, H. Prokisch, L. Xie, Y. Li, H.-E. Wichmann, A. Peters, F. Kronenberg, K. Suhre, J. Adamski, T. Illig, and R. Wang-Sattler, "Differences between human plasma and serum metabolite profiles.," PLoS One, vol. 6, no. 7, p. e21230, Jan. 2011.

[28] G. Janatsch, J. D. Kruse-Jarres, R. Marbach, and H. M. Heise, *"Multivariate calibration for assays in clinical chemistry using attenuated total reflection infrared spectra of human blood plasma,"* Anal. Chem., vol. 61, no. 18, pp. 2016–2023, Sep. 1989.

[29] D. Naumann, *"FT-INFRARED AND FT-RAMAN SPECTROSCOPY IN BIOMEDICAL RESEARCH,"* Appl. Spectrosc. Rev., vol. 36, no. 2–3, pp. 239–298, Jun. 2001.

[30] R. Shaw and H. Mantsch, *"Infrared spectroscopy in clinical and diagnostic analyses,"* Encyclopedia of Analytical Chemistry. John Wiley & Sons, Ltd, 2000.

[31] D. Finkenthal, *Introduction to the electromagnetic spectrum*. General Atomics, 1996.

[32] B. C. Smith, Fundamentals of Fourier Transform Infrared Spectroscopy, Second edi. CRC Press, 2011.

[33] A. Nabers, J. Ollesch, J. Schartner, C. Kötting, J. Genius, U. Haußmann, H. Klafki, J. Wiltfang, and K. Gerwert, *"An infrared sensor analysing label-free the secondary structure of the Abeta peptide in presence of complex fluids,"* J. Biophotonics, 2015.

[34] P. Carmona and M. Molina, *"Infrared spectroscopic analysis of mononuclear leukocytes in peripheral blood from Alzheimer's disease patients,"* Anal. …, vol. 402, no. 6, pp. 2015–21, Feb. 2012.

[35] P. Carmona, M. Molina, M. Calero, F. Bermejo-Pareja, P. Martínez-Martín, and A. Toledano, *"Discrimination analysis of blood plasma associated with Alzheimer's disease using vibrational spectroscopy.,"* J. Alzheimers. Dis., vol. 34, no. 4, pp. 911–20, Jan. 2013.

[36] E. Ryzhikova, O. Kazakov, L. Halamkova, D. Celmins, P. Malone, E. Molho, E. A. Zimmerman, and I. K. Lednev, *"Raman spectroscopy of blood serum for Alzheimer's disease diagnostics: specificity relative to other types of dementia,"* J. Biophotonics, 2014.

[37] P. Chen, Q. Tian, S. J. Baek, X. L. Shang, A. Park, Z. C. Liu, X. Q. Yao, J. Z. Wang, X. H. Wang, Y. Cheng, J. Peng, A. G. Shen, and J. M. Hu, *"Laser Raman detection of platelet as a non-invasive approach for early and differential diagnosis of Alzheimer's disease,"* Laser Phys. Lett., vol. 8, no. 7, pp. 547–552, 2011.

[38] E. Peuchant, S. Richard-Harston, I. Bourdel-Marchasson, J.-F. Dartigues, L. Letenneur, P. Barberger-Gateau, S. Arnaud-Dabernat, and J.-Y. Daniel, *"Infrared spectroscopy: a reagent-free method to distinguish Alzheimer's disease patients from normal-aging subjects.,"* Transl. Res., vol. 152, no. 3, pp. 103–12, Sep. 2008.

[39] H. Komatsu, L. Liu, I. V. J. Murray, and P. H. Axelsen*, "A mechanistic link between oxidative stress and membrane mediated amyloidogenesis revealed by infrared spectroscopy,"* Biochim. Biophys. Acta - Biomembr., vol. 1768, no. 8, pp. 1913–1922, 2007.

[40] H. M. Schipper, C. S. Kwok, S. M. Rosendahl, D. Bandilla, O. Maes, C. Melmed, D. Rabinovitch, and D. H. Burns*, "Spectroscopy of human plasma for diagnosis of idiopathic Parkinson's disease.,"* Biomark. Med., vol. 2, no. 3, pp. 229–238, 2008.

[41] S. Tak, S. J. Yoon, J. Jang, K. Yoo, Y. Jeong, and J. C. Ye, *"Quantitative analysis of hemodynamic and metabolic changes in subcortical vascular dementia using simultaneous near-infrared spectroscopy and fMRI measurements,"* Neuroimage, vol. 55, no. 1, pp. 176–184, 2011.

[42] S. D. Smolarek, *"UV and IR laser spectroscopy of isolated molecular structural dynamics,"* FNWI: Van 't Hoff Institute for Molecular Sciences (HIMS), 2011.

[43] S. Kumar, S. Chaudhary, and D. C. Jain, *"Vibrational Studies of Different Human Body Disorders Using FTIR Spectroscopy,"* Open J. Appl. Sci., vol. 04, no. 03, pp. 103–129, 2014.

[44] A. Barth and P. I. Harris, Eds., *Biological and Biomedical Infrared Spectroscopy.* IOS Press, 2009.

[45] P. Garidel and H. Schott, *"Fourier-Transform Midinfrared Spectroscopy for Analysis and Screening of Liquid Protein Formulations Part 2: Details Analysis and Applications,"* Bioprocess Int., vol. 1, pp. 48–55, 2006.

[46] D. I. Ellis, G. G. Harrigan, and R. Goodacre, *Metabolic Profiling: Its Role in Biomarker Discovery and Gene Function Analysis*. Boston, MA: Springer US, 2003.

[47] L. K. Tamm and S. A. Tatulian, *"Infrared spectroscopy of proteins and peptides in lipid bilayers.,"* Q. Rev. Biophys., vol. 30, no. 4, pp. 365–429, Nov. 1997.

[48] F. Severcan and P. I. Harris*, Vibrational Spectroscopy in Diagnosis and Screening*. IOS Press, 2012.

[49] A. Jabs, *"Determination of Secondary Structure in Proteins by Fourier Transform Infrared Spectroscopy (FTIR),"* 10-Jul-2005. [Online]. Available: http://jenalib.fli-leibniz.de/ImgLibDoc/ftir/IMAGE_FTIR.html. [Accessed: 01-Jan-2014].

[50] A. Barth, *"The infrared absorption of amino acid side chains.," Prog. Biophys. Mol. Biol.*, vol. 74, no. 3–5, pp. 141–73, Jan. 2000.

[51] Tasumi , M., & Sakamoto, A. (2014). *Introduction to Experimental Infrared Spectroscopy: Fundamentals and Practical Methods* (1º ed.). John Wiley & Sons, Ltd.

[52] University of Colorado, Boulder, Dept of Chem and Biochem., *"Infrared spectroscopy: theory,"* in Handbook for Organic Chemistry Lab, 2002, pp. 155–164.

[53] B. H. Stuart, *Infrared Spectroscopy: Fundamentals and Applications*. Chichester, UK: John Wiley & Sons, Ltd, 2004.

[54] Thermo Nicolet Corporation, *"Introduction to Fourier Transform Infrared Spectrometry,"* 2001.

[55] ChemWiki: The Dynamic Chemistry Hypertext; available online: http://chemwiki.ucdavis.edu/Physical_Chemistry/Spectroscopy/Vibrational_Spectroscopy/Infrared_Spectroscopy/Infrared%3A_Theory

[56] J. Coates, *"Interpretation of Infrared Spectra , A Practical Approach,"* Encyclopedia of Analytical Chemistry. John Wiley & Sons Ltd, pp. 10815–10837, 2000.

[57] Sheffield Hallam University, *"Infra-Red Absorption Spectroscopy Theoretical Principles."* [Online]. Available: http://teaching.shu.ac.uk/hwb/chemistry/tutorials/molspec/irspec1.htm.

[58] C. Petibois, G. Cazorla, a Cassaigne, and G. Déléris, *"Plasma protein contents determined by Fourier-transform infrared spectrometry.,"* Clin. Chem., vol. 47, no. 4, pp. 730–8, Apr. 2001.

[59] Specac, *"Specac Product Catalogue 2013."* 2013.

[60] PerkinElmerInc., *"FT-IR Spectroscopy Attenuated Total Reflectance (ATR),"* 2005.

[61] Z. Yu, G. Kastenmüller, Y. He, P. Belcredi, G. Möller, C. Prehn, J. Mendes, S. Wahl, W. Roemisch-Margl, U. Ceglarek, A. Polonikov, N. Dahmen, H. Prokisch, L. Xie, Y. Li, H.-E. Wichmann, A. Peters, F. Kronenberg, K. Suhre, J. Adamski, T. Illig, and R. Wang-Sattler, *"Differences between human plasma and serum metabolite profiles.,"* PLoS One, vol. 6, no. 7, p. e21230, Jan. 2011.

[62] R. Shaw and H. Mantsch, *"Infrared spectroscopy in clinical and diagnostic analyses,"* Encyclopedia of Analytical Chemistry. John Wiley & Sons, Ltd, 2000.

[63] R. Cerdeira Silva, *"Identification of Alzheimer biomarkers by FTIR - a pilot study,"* University of Aveiro, 2013.

[64] M. S. S. Correia, "Identification of potential Alzheimer's disease biomarkers in plasma using FTIR " University of Aveiro, 2014.

[65] Larkin P. *Infrared and Raman Spectroscopy: Principles and Interpretation*. Elsevier; 2011.

[66] Lee S, Mirkin NG. *A quantitative anharmonic analysis of the amide A band in α-helical poly(L-alanine)*. Biopolymers. 1999, 49(3): 195-207

[67] Delenis G, Petibois C. *Applications of FT-IR spectrometry to plasma contents analysis and monitoring*. Vibrational Spectroscopy. 2003; 32(1): 129-36

[68] Coates J. *Interpretation of Infrared Spectra, A Practical Approach Interpretation of Infrared Spectra*. In: Meyers RA, editor. Encyclopedia of Analytical Chemestry. John Wiley & Sons Ltd; 2000.

[69] Thirunavukkarasu M. *FTIR and uv-visible spectral study on normal blood samples.* IJPBS. 2011; 1(2)

[70] Barth A, Zscherp C. *What vibrations tell about proteins*. Quaterly Reviews of Biophysiscs. 2002 Nov; 35(4): 369-430

[71] Kong J, Yu S. *Fourier Transform Infrared Spectroscopic Analysis of Protein Secondary Structures*. Acta Biochimica Biophysica Sinica. 2007; 39(8): 549-59

[72] Davis R, Mauer LJ. *Fourier transform infrared (FT-IR) spectroscopy: a rapid tool for detection and analysis of foodborne pathogenic bacteria*. 2010; (1): 1582-94.

[73] Movasaghi Z, Rehman S, ur Rehman DI. *Fourier Transform Infrared (FTIR) Spectroscopy of Biological tissues.* Applied Spectroscopy Reviews. 2008 Feb; 43(2): 134-79

[74] Kannemeier C, Shibamiya A, Nakazawa F, Trusheim H, Ruppert C, Markart P, et al. *Extracellular RNA constitutes a natural procoagulant cofactor in blood coagulation. Proceedings of the National Academy of Sciences of the United States of America.* 2007Apr 10; 104(15): 6388-93

[75] Van der Meijden PEJ, Munnix IC a, Auger JM, Govers-Riemslag JWP, Cosemans JMEM, Kuijpers MJE, et al. *Dual role of collagen in factor XII- dependent thrombus formation.* Blood. 2009 Jul 23; 114(4): 881-90

[76] D. I. Ellis, G. G. Harrigan, and R. Goodacre, "*Metabolic Profiling: Its Role in Biomarker Discovery and Gene Function Analysis.*" Boston, MA: Springer US, 2003, pp. 111–124.

[77] D. Naumann, *"FT-INFRARED AND FT-RAMAN SPECTROSCOPY IN BIOMEDICAL RESEARCH,"* Appl. Spectrosc. Rev., vol. 36, no. 2–3, pp. 239–298, Jun. 2001.

[78] G. Basurto-Islas and K. Iqbal, *"A molecular mechanism by which acidosis of the brain can lead to Alzheimer's disease," Alzheimer's Dement.*, vol. 9, no. 4, p. P307, Jul. 2013.

[79] A. C. Leskovjan, A. Kretlow, and L. M. Miller, *"Fourier transform infrared imaging showing reduced unsaturated lipid content in the hippocampus of a mouse model of Alzheimer's disease.," Anal. Chem.*, vol. 82, no. 7, pp. 2711–6, Apr. 2010.

[80] V. Dritsa, *"FT-IR Spectroscopy in Medicine,"* in *Infrared Spectroscopy - Life and Biomedical Sciences*, T. Theophile, Ed. InTech, 2012, pp. 271–288.

[81] M. J. Calkins, D. A. Johnson, J. A. Townsend, M. R. Vargas, J. A. Dowell, T. P. Williamson, A. D. Kraft, J.-M. Lee, J. Li, and J. A. Johnson, *"The Nrf2/ARE pathway as a potential therapeutic target in neurodegenerative disease.," Antioxid. Redox Signal.*, vol. 11, no. 3, pp. 497–508, Mar. 2009.

[82] B. Shivu, S. Seshadri, J. Li, K. A. Oberg, V. N. Uversky, and A. L. Fink, *"Distinct β-sheet structure in protein aggregates determined by ATR-FTIR spectroscopy.," Biochemistry*, vol. 52, no. 31, pp. 5176–83, Aug. 2013.

[83] E. Cerf, R. Sarroukh, S. Tamamizu-Kato, L. Breydo, S. Derclaye, Y. F. Dufrêne, V. Narayanaswami, E. Goormaghtigh, J.-M. Ruysschaert, and V. Raussens, *"Antiparallel beta-sheet: a signature structure of the oligomeric amyloid beta-peptide.," Biochem. J.*, vol. 421, no. 3, pp. 415–23, Aug. 2009.

[84] N. Kanagathara, M. Thirunavukkarasu, E. Jeyanthi C, and P. Shenbagarajan*, "FTIR AND UV-VISIBLE SPECTRAL STUDY ON NORMAL BLOOD SAMPLES," Int. J. Pharm. Biol. Sci.*, vol. 1, no. 2, pp. 74–81, 2011.

[85] F. Rincon and C. B. Wright, *“Vascular cognitive impairment.,” Curr. Opin. Neurol.*, vol. 26, no. 1, pp. 29–36, Mar. 2013.